

1 Quasi-consistent efficient meshfree thin shell
2 formulation with penalty-free essential boundary
3 condition enforcement

4 Junchao Wu^{a,*}, Yangtao Xu^a, Bin Xu^a, Syed Humayun Basha^a

^a*Key Laboratory for Intelligent Infrastructure and Monitoring of Fujian Province, Key Laboratory for Structural Engineering and Disaster Prevention of Fujian Province, College of Civil Engineering, Huaqiao University, Xiamen, Fujian, 361021, China*

5 **Abstract**

This research proposed an efficient and quasi-consistent meshfree thin shell formulation with penalty-free enforcement of essential boundary conditions. Within the framework of the Hu-Washizu variational principle, a mixed formulation of displacements, strains and stresses is employed in this approach, where the displacements are discretized using meshfree shape functions, and the strains and stresses are expressed using smoothed gradients, covariant smoothed gradients and covariant bases. The smoothed gradients satisfy the first second-order integration constraint and have variational consistency for polynomial strains and stresses. Owing to Hu-Washizu variational principle, the essential boundary conditions automatically arise in its weak form. As a result, the suggested technique's enforcement of essential boundary conditions resembles that of the traditional Nitsche's method. Contrary to Nitsche's method, the costly higher order derivatives of conventional meshfree shape functions were replaced by the smoothed gradients with fast computation, which improve the efficiency. Meanwhile, the proposed formulation features a naturally stabilized term without adding any artificial stabilization factors, which eliminates the employment of penalty method as a stabilization. The efficacy of the proposed Hu-Washizu meshfree thin shell formulation is illustrated by a set of classical standard thin shell problems.

6 *Keywords:* Meshfree, Thin shell, Hu-Washizu variational principle,
7 Reproducing kernel gradient smoothing, Essential boundary condition

*Corresponding author
Email address: jcwu@hqu.edu.cn (Junchao Wu)

8 **1. Introduction**

9 Thin shell structures generally adhere to the Kirchhoff hypothesis [1], that
10 neglects the shear deformation can be described using Galerkin formulation
11 which requires to have at least C^1 continuity. The traditional finite element
12 methods usually have C^0 continuous shape functions, and it prefers Mindlin
13 thick shear theory, hybrid and mixed models in simulation of shell structure [2].
14 Meshfree methods [3, 4, 5] with high order smoothed shape functions have gar-
15 nered much research attention over the past thirty years. These techniques es-
16 tablished the shape functions based on a collection of dispersed nodes, and high
17 order continuity of shape functions can be easily achieved even with low-order
18 basis functions. For thin shell analysis, high order meshfree approximation can
19 also furhter alleviate the membrane locking caused by the mismatched approxi-
20 mation order of membrane strain and bending strain [6]. Moreover, nodal-based
21 meshfree approximations generally offer the flexibility of local refinement and
22 can relieve the burden of mesh distortion. Owing to these benefits, numerous
23 meshfree techniques have been developed and implemented in many scientific
24 and engineering fields [7, 8, 9, 10, 11, 12, 13]. However, the high order smoothed
25 meshfree shape functions accompany the enlarged and overlapping supports,
26 which may potentially cause many problems for shape functions. One of the
27 issues is the loss of the Kronecker delta property, which means that, unlike the
28 finite element methods, the necessary boundary conditions cannot be directly
29 enforced [14]. Another issue is that the variational consistency or said integra-
30 tion constraint, which is a condition that requires the formulation to exactly
31 reproduce the solution spanned by the basis functions, cannot be satisfied. This
32 issue is mainly caused by the misalignment between the numerical integration
33 domains and supports of shape functions. Thus, the shape functions exhibit a
34 piecewise nature in each integration domain. Besides, it has to be noted that
35 the traditional integration rules like Gauss scheme cannot ensure the integration
36 accuracy in Galerkin weak form [15, 16]. Therefore, variational consistency is
37 vital to the solution accuracy in the Galerkin meshfree formulations.

38 Various ways have been presented to enforce the necessary boundary for
39 Galerkin meshfree methods directly, including the boundary singular kernel
40 method [17], mixed transformation method [17], and interpolation element-free
41 method [18] for recovering shape functions' Kronecker property. However, these
42 methods were not based on variational setting and cannot guarantee variational
43 consistency. In the absence of a meshfree node, accuracy enforcement might be
44 poor. In contrast, enforcing the essential boundary conditions using a variational
45 approach is preferred for Galerkin meshfree methods. The variational consis-
46 tent Lagrange multiplier approach was initially used to the Galerkin meshfree
47 method by Belytschko et al. [3]. In this method, the extra degrees of freedom
48 are used to determine the discretion of Lagrange multiplier. Ivannikov et al. [19]
49 extended this approach to geometrically nonlinear thin shells. Lu et al. [20] sug-
50 gested the modified variational essential boundary enforcement approach and
51 expressed the Lagrange multiplier by equivalent tractions to eliminate the ex-
52 cess degrees of freedom. However, the coercivity of this approach is not always

ensured and potentially reduces the accuracy. Zhu and Atluri [21] pioneered the penalty method for meshfree method, making it a straightforward approach to enforce essential boundary conditions via Galerkin weak form. However, the penalty method lacks variational consistency and requires experimental artificial parameters whose optimal value is hard to determine. Fernández-Méndez and Huerta [14] imposed necessary boundary conditions using Nitsche's approach in the meshfree formulation. This approach can be seen as a hybrid combination of the modified variational method and the penalty method because the modified variational method generates variational consistency through the use of a consistent term, and the penalty method is used as a stabilized term to recover the coercivity. Skatulla and Sansour [22] extended Nitsche's thin shell analysis method and proposed an iteration algorithm to determine artificial parameters at each integration point.

In order to address the issue of numerical integration, a series of consistent integration schemes have been developed for Galerkin meshfree methods. Among these include stabilized conforming nodal integration [23], variational consistent integration [24], quadratic consistent integration [25], reproducing kernel gradient smoothing integration [26], and consistent projection integration [27]. The assumed strain approach establishes the most consistent integration scheme, while the smoothed gradient replaces the costly higher order derivatives of traditional meshfree shape functions and shows a high efficiency. Moreover, to achieve global variational consistency, a consistent essential boundary condition enforcement must be combined with the consistent integration scheme. The combination of consistent integration scheme and Nitsche's method for treating essential boundary conditions may demonstrate better performance since both the methods can satisfy the coercivity without requiring additional degrees of freedom. Nevertheless, Nitsche's approach still retains the artificial parameters in the stabilized terms, and it is essential to remain cautious of the costly higher order derivatives, particularly for thin plate and thin shell problems. Recently, Wu et al. [28, 29] proposed an efficient and stabilized essential boundary condition enforcement method based upon the Hellinger-Reissner variational principle, where a mixed formulation in Hellinger-Reissner weak form recasts the reproducing kernel gradient smoothing integration. The terms required for enforcing essential boundary conditions are identical to the Nitsche's method, and both have consistent and stabilized terms. However, the stabilized term of this method naturally exists in the Hellinger-Reissner weak form and no longer needs the artificial parameters, even for essential boundary enforcement. Instead all of the higher order derivatives are represented by the smoothed gradients and their derivatives.

In this study, an efficient and stabilized variational consistent meshfree method that naturally enforces the essential boundary conditions is developed for thin shell structures. Following the concept of the Hellinger-Reissner principle base consistent meshfree method, the Hu-Washizu variational principle of complementary energy with variables of displacement, strains, and stresses were employed. The displacement is approximated by conventional meshfree shape functions, and the strains and stresses were expressed by smoothed gradients

99 with covariant bases. It is important to note that although the first second-order
100 integration requirements were naturally embedded in the smoothed gradients,
101 their fulfillment resulted in a quasi-satisfaction of variational consistency. This
102 is mainly because of the non-polynomial nature of the stresses. Hu-Washizu's
103 weak form was used to evaluate all the essential boundary conditions regard-
104 ing displacements and rotations. This type of formulation is similar to the
105 Nitsche's method but does not require any artificial parameters. Compared
106 with Nitsche's method, conventional reproducing smoothed gradients and its
107 direct derivatives replace the costly higher order derivatives. By utilizing the
108 advantages of a replicating kernel gradient smoothing framework, the smoothed
109 gradients showed better performance compared to conventional derivatives of
110 shape functions, hence increasing the meshfree formulation's computational ef-
111 ficiency.

112 The remainder of this research article is structured as follows: The kinemat-
113 ics of the thin shell structure and the weak form of the associated Hu-Washizu
114 principle are briefly described in Section 2. Subsequently, the mixed formulation
115 regarding the displacements, strains and stresses in accordance with Hu-Washizu
116 weak form are presented in Section 3. The discrete equilibrium equations are
117 derived in Section 4 using the naturally occurring accommodation of essen-
118 tial. Subsequently, they are compared to the equations obtained using Nitsche's
119 method. The numerical results in Section 5 validate the efficacy of the proposed
120 Hu-Washizu meshfree thin shell formulation. Lastly, the concluding remarks are
121 presented in Section 6.

¹²² **2. Hu-Washizu's formulation of complementary energy for thin shell**

¹²³ *2.1. Kinematics for thin shell*

¹²⁴ Consider the configuration of a shell $\bar{\Omega}$, as shown in Fig. 1, which can be
¹²⁵ easily described by a parametric curvilinear coordinate system $\xi = \{\xi^i\}_{i=1,2,3}$.
¹²⁶ The mid-surface of the shell denoted by Ω is specified by the in-plane coordinates
¹²⁷ $\xi = \{\xi^\alpha\}_{\alpha=1,2}$, as the thickness direction of shell is by ξ^3 , $-\frac{h}{2} \leq \xi^3 \leq \frac{h}{2}$, h is
¹²⁸ the thickness of shell. In this work, Latin indices take the values from 1 to 3,
¹²⁹ and Greek indices are evaluated by 1 or 2. For the Kirchhoff hypothesis [6], the
¹³⁰ position $\mathbf{x} \in \bar{\Omega}$ is defined by linear functions with respect to ξ^3 :

$$\mathbf{x}(\xi^1, \xi^2, \xi^3) = \mathbf{r}(\xi^1, \xi^2) + \xi^3 \mathbf{a}_3(\xi^1, \xi^2) \quad (1)$$

in which \mathbf{r} means the position on the mid-surface of shell, and \mathbf{a}_3 is correspond-

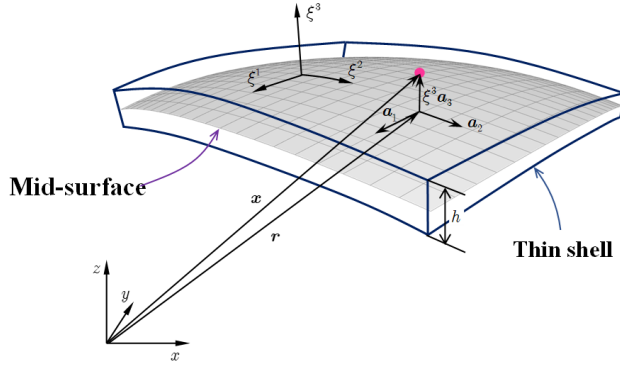


Figure 1: Kinematics for thin shell.

¹³¹
¹³² ing normal direction. For the mid-surface of shell, the in-plane covariant base
¹³³ vector with respect to ξ^α can be derived by a trivial partial differentiation to \mathbf{r} :

$$\mathbf{a}_\alpha = \frac{\partial \mathbf{r}}{\partial \xi^\alpha} = \mathbf{r}_{,\alpha}, \alpha = 1, 2 \quad (2)$$

¹³⁴ to provide for a clear expression, the subscript comma denotes the partial dif-
¹³⁵ ferentiation operation with respect to in-plane coordinates ξ^α , and the normal
¹³⁶ vector \mathbf{a}_3 can be obtained by the normalized cross product of \mathbf{a}_α 's as follows:

$$\mathbf{a}_3 = \frac{\mathbf{a}_1 \times \mathbf{a}_2}{\|\mathbf{a}_1 \times \mathbf{a}_2\|} \quad (3)$$

¹³⁷ where $\|\bullet\|$ is the Euclidean norm operator.

¹³⁸ With the assumption of infinitesimal deformation, the strain components
¹³⁹ with respect to the global contravariant base can be stated as:

$$\epsilon_{ij} = \frac{1}{2} (\mathbf{x}_{,i} \cdot \mathbf{u}_{,j} + \mathbf{u}_{,i} \cdot \mathbf{x}_{,j}) \quad (4)$$

¹⁴⁰ where \mathbf{u} represents the displacement for the shell deformation. To satisfy the
¹⁴¹ Kirchhoff hypothesis, the displacement is assumed to be of the following form:

$$\mathbf{u}(\xi^1, \xi^2, \xi^3) = \mathbf{v}(\xi^1, \xi^2) + \boldsymbol{\theta}(\xi^1, \xi^2)\xi^3 \quad (5)$$

¹⁴² in which the quadratic and higher order terms are neglected. $\mathbf{v}, \boldsymbol{\theta}$ represent
¹⁴³ the displacement and rotation in mid-surface, respectively.

¹⁴⁴ Subsequently, plugging Eqs. (1) and (5) into Eq. (4) and neglecting the
¹⁴⁵ quadratic terms, the strain components can be rephrased as follows:

$$\begin{aligned} \epsilon_{\alpha\beta} &= \frac{1}{2}(\mathbf{a}_\alpha \cdot \mathbf{v}_{,\beta} + \mathbf{v}_{,\alpha} \cdot \mathbf{a}_\beta) \\ &\quad + \frac{1}{2}(\mathbf{a}_{3,\alpha} \cdot \mathbf{v}_{,\beta} + \mathbf{v}_{,\alpha} \cdot \mathbf{a}_{3,\beta} + \mathbf{a}_\alpha \cdot \boldsymbol{\theta}_{,\beta} + \boldsymbol{\theta}_{,\alpha} \cdot \mathbf{a}_\beta)\xi^3 \end{aligned} \quad (6a)$$

$$\epsilon_{\alpha 3} = \frac{1}{2}(\mathbf{a}_\alpha \cdot \boldsymbol{\theta} + \mathbf{v}_{,\alpha} \cdot \mathbf{a}_3) + \frac{1}{2}(\mathbf{a}_3 \cdot \boldsymbol{\theta})_{,\alpha}\xi^3 \quad (6b)$$

$$\epsilon_{33} = \mathbf{a}_3 \cdot \boldsymbol{\theta} \quad (6c)$$

¹⁴⁶ where $\epsilon_{\alpha\beta}, \kappa_{\alpha\beta}$ represent membrane and bending strains, respectively, and are
¹⁴⁷ given as follows:

$$\epsilon_{\alpha\beta} = \frac{1}{2}(\mathbf{a}_\alpha \cdot \mathbf{v}_{,\beta} + \mathbf{v}_{,\alpha} \cdot \mathbf{a}_\beta) \quad (7)$$

$$\kappa_{\alpha\beta} = \frac{1}{2}(\mathbf{a}_{3,\alpha} \cdot \mathbf{v}_{,\beta} + \mathbf{v}_{,\alpha} \cdot \mathbf{a}_{3,\beta} + \mathbf{a}_\alpha \cdot \boldsymbol{\theta}_{,\beta} + \boldsymbol{\theta}_{,\alpha} \cdot \mathbf{a}_\beta) \quad (8)$$

¹⁴⁹ In accordance with the Kirchhoff hypothesis, the thickness of shell will not
¹⁵⁰ change, and the deformation related with direction of ξ^3 will vanish, i.e. $\epsilon_{3i} = 0$.
¹⁵¹ Thus, the rotation $\boldsymbol{\theta}$ can be rewritten as:

$$\epsilon_{3i} = 0 \Rightarrow \begin{cases} \boldsymbol{\theta} \cdot \mathbf{a}_\alpha = -\mathbf{v}_{,\alpha} \cdot \mathbf{a}_3 \\ \boldsymbol{\theta} \cdot \mathbf{a}_3 = 0 \end{cases} \Rightarrow \boldsymbol{\theta} = -\mathbf{v}_{,\alpha} \cdot \mathbf{a}_3 \mathbf{a}^\alpha \quad (9)$$

¹⁵² where \mathbf{a}^α 's is the in-plane contravariant base vector, $\mathbf{a}^\alpha \cdot \mathbf{a}_\beta = \delta_\beta^\alpha$, δ is the
¹⁵³ Kronecker delta function. The detailed derivation of Eq. 9 can be found in
¹⁵⁴ reference [30].

¹⁵⁵ Furthermore, substituting Eq. (9) into Eq. (8) leads to:

$$\kappa_{\alpha\beta} = (\Gamma_{\alpha\beta}^\gamma \mathbf{v}_{,\gamma} - \mathbf{v}_{,\alpha\beta}) \cdot \mathbf{a}_3 = -\mathbf{v}_{,\alpha\beta} \cdot \mathbf{a}_3 \quad (10)$$

¹⁵⁶ in which $\Gamma_{\alpha\beta}^\gamma = \mathbf{a}_{\alpha,\beta} \cdot \mathbf{a}^\gamma$ is namely the Christoffel symbol of the second kind,
¹⁵⁷ and $\mathbf{v}_{,\alpha\beta}$ is the in-plane covariant derivative of $\mathbf{v}_{,\alpha}$, i.e. $\mathbf{v}_{,\alpha\beta} = \Gamma_{\alpha\beta}^\gamma \mathbf{v}_{,\gamma} - \mathbf{v}_{,\alpha\beta}$.

¹⁵⁸ 2.2. Galerkin weak form for Hu-Washizu principle of complementary energy

¹⁵⁹ In this study, the Hu-Washizu variational principle of complementary energy
¹⁶⁰ [31] was adopted for the development of the proposed analytical approach, the

¹⁶¹ corresponding complementary functional, denoted by Π_C , is listed as follows:

$$\begin{aligned} & \Pi_C(\varepsilon_{\alpha\beta}, \kappa_{\alpha\beta}, N^{\alpha\beta}, M^{\alpha\beta}) \\ &= \int_{\Omega} \frac{h}{2} \varepsilon_{\alpha\beta} C^{\alpha\beta\gamma\eta} \varepsilon_{\gamma\eta} d\Omega + \int_{\Omega} \frac{h^3}{24} \kappa_{\alpha\beta} C^{\alpha\beta\gamma\eta} \kappa_{\gamma\eta} d\Omega \\ &+ \int_{\Omega} \varepsilon_{\alpha\beta} (N^{\alpha\beta} - h C^{\alpha\beta\gamma\eta} \varepsilon_{\gamma\eta}) d\Omega + \int_{\Omega} \kappa_{\alpha\beta} (M^{\alpha\beta} - \frac{h^3}{12} C^{\alpha\beta\gamma\eta} \kappa_{\gamma\eta}) d\Omega \\ &- \int_{\Gamma_v} \mathbf{T} \cdot \bar{\mathbf{v}} d\Gamma + \int_{\Gamma_\theta} M_{\mathbf{n}\mathbf{n}} \bar{\theta}_{\mathbf{n}} d\Gamma - (P \mathbf{a}_3 \cdot \bar{\mathbf{v}})_{\mathbf{x} \in C_w} \end{aligned} \quad (11)$$

¹⁶² where $C^{\alpha\beta\gamma\eta}$'s represent the components of fourth order elasticity tensor with
¹⁶³ respect to the covariant base and plane stress assumption, and it can be ex-
¹⁶⁴ pressed by Young's modulus E , Poisson's ratio ν and the in-plane contravariant
¹⁶⁵ metric coefficients $a^{\alpha\beta}$'s, $a^{\alpha\beta} = \mathbf{a}^\alpha \cdot \mathbf{a}^\beta$, as follows:

$$C^{\alpha\beta\gamma\eta} = \frac{E}{2(1+\nu)} (a^{\alpha\gamma} a^{\beta\eta} + a^{\alpha\eta} a^{\beta\gamma} + \frac{2\nu}{1-\nu} a^{\alpha\beta} a^{\gamma\eta}) \quad (12)$$

¹⁶⁶ and $N^{\alpha\beta}$, $M^{\alpha\beta}$ represent the components of membrane- and bending- stresses
¹⁶⁷ which are given by:

$$N^{\alpha\beta} = h C^{\alpha\beta\gamma\eta} \varepsilon_{\gamma\eta}, \quad M^{\alpha\beta} = \frac{h^3}{12} C^{\alpha\beta\gamma\eta} \kappa_{\gamma\eta} \quad (13)$$

¹⁶⁸ Essential boundaries on the edges and corners denoted by Γ_v , Γ_θ and C_v
¹⁶⁹ are naturally existed in complementary energy functional, and $\bar{\mathbf{v}}$, $\bar{\theta}_{\mathbf{n}}$ are the
¹⁷⁰ corresponding prescribed displacement and normal rotation, respectively. \mathbf{T} ,
¹⁷¹ $M_{\mathbf{n}\mathbf{n}}$ and P can be determined by Euler-Lagrange equations of shell problem
¹⁷² [30] as follows:

$$\mathbf{T} = \mathbf{T}_N + \mathbf{T}_M \rightarrow \begin{cases} \mathbf{T}_N = \mathbf{a}_\alpha N^{\alpha\beta} n_\beta \\ \mathbf{T}_M = (\mathbf{a}_3 M^{\alpha\beta} s_\alpha n_\beta)_{,\gamma} s^\gamma + (\mathbf{a}_3 M^{\alpha\beta})|_\beta n_\alpha \end{cases} \quad (14)$$

$$M_{\mathbf{n}\mathbf{n}} = M^{\alpha\beta} n_\alpha n_\beta \quad (15)$$

$$P = -[[M^{\alpha\beta} s_\alpha n_\beta]] \quad (16)$$

¹⁷⁵ where $\mathbf{n} = n^\alpha \mathbf{a}_\alpha = n_\alpha \mathbf{a}^\alpha$ and $\mathbf{s} = s^\alpha \mathbf{a}_\alpha = s_\alpha \mathbf{a}^\alpha$ are the outward normal and
¹⁷⁶ tangent directions on boundaries. $[[f]]$ is the jump operator defined by:

$$[[f]]_{\mathbf{x}=\mathbf{x}_c} = \lim_{\epsilon \rightarrow 0^+} (f(\mathbf{x}_c + \epsilon) - f(\mathbf{x}_c - \epsilon)), \mathbf{x}_c \in \Gamma \quad (17)$$

¹⁷⁷ where f is an arbitrary function on Γ .

¹⁷⁸ Moreover, the natural boundary conditions should be applied by Lagrangian
¹⁷⁹ multiplier method with displacement \mathbf{v} regarded as multiplier. Thus, then the

¹⁸⁰ new complementary energy functional namely Π is given by:

$$\begin{aligned} & \Pi(\mathbf{v}, \varepsilon_{\alpha\beta}, \kappa_{\alpha\beta}, N^{\alpha\beta}, M^{\alpha\beta}) \\ &= \Pi_C(\varepsilon_{\alpha\beta}, \kappa_{\alpha\beta}, N^{\alpha\beta}, M^{\alpha\beta}) + \int_{\Gamma_M} \theta_n (M_{nn} - \bar{M}_{nn}) d\Gamma \\ & \quad - \int_{\Gamma_T} \mathbf{v} \cdot (\bar{\mathbf{T}}) d\Gamma - \mathbf{v} \cdot \mathbf{a}_3 (P - \bar{P})_{x \in C_P} - \int_{\Omega} \mathbf{v} \cdot (\bar{\mathbf{b}}) d\Omega \end{aligned} \quad (18)$$

¹⁸¹ where $\bar{\mathbf{T}}$, \bar{M}_{nn} and \bar{P} are the prescribed traction, bending moment and concentrated force on the edges Γ_T , Γ_M and corner C_P , respectively. All the specified boundaries meet the following geometric relationships:

$$\begin{cases} \Gamma = \Gamma_v \cup \Gamma_T \cup \Gamma_\theta \cup \Gamma_M, & C = C_v \cup C_P, \\ \Gamma_v \cap \Gamma_T = \Gamma_\theta \cap \Gamma_M = C_v \cap C_P = \emptyset \end{cases} \quad (19)$$

¹⁸⁴ and $\bar{\mathbf{b}}$ stands for the prescribed body force in Ω , \mathbf{b} can be written based on
¹⁸⁵ Euler-Lagrange equations [30] as:

$$\mathbf{b} = \mathbf{b}_N + \mathbf{b}_M \rightarrow \begin{cases} \mathbf{b}_N = (\mathbf{a}_\alpha N^{\alpha\beta})|_\beta \\ \mathbf{b}_M = (\mathbf{a}_3 M^{\alpha\beta})|_{\alpha\beta} \end{cases} \quad (20)$$

¹⁸⁶ Introducing a standard variational argument to Eq. (18), $\delta\Pi = 0$, and
¹⁸⁷ considering the arbitrariness of virtual variables, $\delta\mathbf{v}$, $\delta\varepsilon_{\alpha\beta}$, $\delta\kappa_{\alpha\beta}$, $N^{\alpha\beta}$, $M^{\alpha\beta}$
¹⁸⁸ lead to the following weak form:

$$-\int_{\Omega} h \delta \varepsilon_{\alpha\beta} C^{\alpha\beta\gamma\eta} \varepsilon_{\gamma\eta} d\Omega + \int_{\Omega} \delta \varepsilon_{\alpha\beta} N^{\alpha\beta} d\Omega = 0 \quad (21a)$$

$$-\int_{\Omega} \frac{h^3}{12} \delta \kappa_{\alpha\beta} C^{\alpha\beta\gamma\eta} \kappa_{\gamma\eta} d\Omega + \int_{\Omega} \delta \kappa_{\alpha\beta} M^{\alpha\beta} d\Omega = 0 \quad (21b)$$

$$\begin{aligned} \int_{\Omega} \delta N^{\alpha\beta} \varepsilon_{\alpha\beta} d\Omega - \int_{\Gamma} \delta \mathbf{T}_N \cdot \mathbf{v} d\Gamma + \int_{\Omega} \delta \mathbf{b}_N \cdot \mathbf{v} d\Omega \\ + \int_{\Gamma_v} \delta \mathbf{T}_N \cdot \mathbf{v} d\Gamma = \int_{\Gamma_v} \delta \mathbf{T}_N \cdot \bar{\mathbf{v}} d\Gamma \end{aligned} \quad (21c)$$

$$\begin{aligned} \int_{\Omega} \delta M^{\alpha\beta} \kappa_{\alpha\beta} d\Omega - \int_{\Gamma} \delta M_{nn} \theta_n d\Gamma + \int_{\Gamma} \delta \mathbf{T}_M \cdot \mathbf{v} d\Gamma + (\delta P \mathbf{a}_3 \cdot \mathbf{v})_{x \in C} + \int_{\Omega} \delta \mathbf{b}_M \cdot \mathbf{v} d\Omega \\ + \int_{\Gamma_\theta} \delta M_{nn} \theta_n d\Gamma - \int_{\Gamma_v} \delta \mathbf{T}_M \cdot \mathbf{v} d\Gamma - (\delta P \mathbf{a}_3 \cdot \mathbf{v})_{x \in C_v} \\ = \int_{\Gamma_\theta} \delta M_{nn} \bar{\theta}_n d\Gamma - \int_{\Gamma_v} \delta \mathbf{T}_M \cdot \bar{\mathbf{v}} d\Gamma - (\delta P \mathbf{a}_3 \cdot \bar{\mathbf{v}})_{x \in C_v} \end{aligned} \quad (21d)$$

$$\begin{aligned}
& \int_{\Gamma} \delta \theta_n M_{nn} d\Gamma - \int_{\Gamma} \delta \mathbf{v} \cdot \mathbf{T} d\Gamma - (\delta \mathbf{v} \cdot \mathbf{a}_3 P)_{x \in C} + \int_{\Omega} \delta \mathbf{v} \cdot \mathbf{b} d\Omega \\
& - \int_{\Gamma_\theta} \delta \theta_n M_{nn} d\Gamma + \int_{\Gamma_v} \delta \mathbf{v} \cdot \mathbf{T} d\Gamma + (\delta \mathbf{v} \cdot \mathbf{a}_3 P)_{x \in C_v} = - \int_{\Gamma_T} \delta \mathbf{v} \cdot \bar{\mathbf{t}} d\Gamma - \int_{\Omega} \delta \mathbf{v} \cdot \bar{\mathbf{b}} d\Omega
\end{aligned} \tag{21e}$$

¹⁹³ where the geometric relationships of Eq. (19) is used herein.

194 **3. Mixed meshfree formulation for modified Hellinger-Reissner weak
195 form**

196 *3.1. Reproducing kernel approximation for displacement*

197 This study approximates the displacement by adopting reproducing kernel
198 approximation. As shown in Fig. 2, the mid-surface of the shell Ω is discretized
199 by a set of meshfree nodes $\{\xi_I\}_{I=1}^{n_p}$ in parametric configuration, where n_p is the
200 total number of meshfree nodes. The approximated displacement namely \mathbf{v}^h
201 can be expressed as:

$$\mathbf{v}(\xi) = \sum_{I=1}^{n_p} \Psi_I(\xi) \mathbf{d}_I \quad (22)$$

202 in which Ψ_I and \mathbf{d}_I is the shape function and nodal coefficient tensor related by
203 node ξ_I . According to reproducing kernel approximation [4], the shape function
204 takes the following form:

$$\Psi_I(\xi) = \mathbf{p}^T(\xi) \mathbf{c}(\xi) \phi(\xi_I - \xi) \quad (23)$$

205 where \mathbf{p} is the basis function vector represented using the following quadratic
206 function as:

$$\mathbf{p} = \{1, \xi^1, \xi^2, (\xi^1)^2, \xi^1 \xi^2, (\xi^2)^2\}^T \quad (24)$$

207 The kernel function denoted by ϕ controls the support and smoothness of
208 meshfree shape functions. The quintic B-spline function with square support is
209 used herein as the kernel function:

$$\phi(\xi_I - \xi) = \phi(\hat{s}_1)\phi(\hat{s}_2), \quad \hat{s}_\alpha = \frac{|\xi_I^\alpha - \xi^\alpha|}{s_{\alpha I}} \quad (25)$$

210 with

$$\phi(\hat{s}_\alpha) = \frac{1}{5!} \begin{cases} (3 - 3\hat{s}_\alpha)^5 - 6(2 - 3\hat{s}_\alpha)^5 + 15(1 - 3\hat{s}_\alpha)^5 & \hat{s}_\alpha \leq \frac{1}{3} \\ (3 - 3\hat{s}_\alpha)^5 - 6(2 - 3\hat{s}_\alpha)^5 & \frac{1}{3} < \hat{s}_\alpha \leq \frac{2}{3} \\ (3 - 3\hat{s}_\alpha)^5 & \frac{2}{3} < \hat{s}_\alpha \leq 1 \\ 0 & \hat{s}_\alpha > 1 \end{cases} \quad (26)$$

211 and $s_{\alpha I}$ means the support size of meshfree shape function Ψ_I .

212 The unknown vector \mathbf{c} in shape function are determined by the fulfillment
213 of the so-called consistency condition:

$$\sum_{I=1}^{n_p} \Psi_I(\xi) \mathbf{p}(\xi_I) = \mathbf{p}(\xi) \quad (27)$$

214 or equivalently

$$\sum_{I=1}^{n_p} \Psi_I(\xi) \mathbf{p}(\xi_I - \xi) = \mathbf{p}(\mathbf{0}) \quad (28)$$

²¹⁵ Substituting Eq. (22) into (28), yields:

$$\mathbf{A}(\boldsymbol{\xi})\mathbf{c}(\boldsymbol{\xi}) = \mathbf{p}(\mathbf{0}) \Rightarrow \mathbf{c}(\boldsymbol{\xi}) = \mathbf{A}^{-1}(\boldsymbol{\xi})\mathbf{p}(\mathbf{0}) \quad (29)$$

²¹⁶ where \mathbf{A} is the moment matrix:

$$\mathbf{A}(\boldsymbol{\xi}) = \sum_{I=1}^{n_p} \phi(\boldsymbol{\xi}_I - \boldsymbol{\xi}) \mathbf{p}(\boldsymbol{\xi}_I - \boldsymbol{\xi}) \mathbf{p}^T(\boldsymbol{\xi}_I - \boldsymbol{\xi}) \quad (30)$$

²¹⁷ Substituting Eq. (29) back into Eq. (22), the expression of meshfree shape
²¹⁸ function can be written as:

$$\Psi_I(\boldsymbol{\xi}) = \mathbf{p}^T(\boldsymbol{\xi}_I - \boldsymbol{\xi}) \mathbf{A}^{-1}(\boldsymbol{\xi}) \mathbf{p}(\mathbf{0}) \phi(\boldsymbol{\xi}_I - \boldsymbol{\xi}) \quad (31)$$

²¹⁹ *3.2. Reproducing kernel gradient smoothing approximation for effective stress
²²⁰ and strain*

²²¹ In Galerkin meshfree formulation, the mid-plane of thin shell Ω is split by
²²² a set of integration cells Ω_C 's, $\cup_{C=1}^{n_e} \Omega_C \approx \Omega$, as shown in Fig. 2. With the
²²³ inspiration of reproducing kernel smoothing framework, the Cartesian and co-
²²⁴ variant derivatives of displacement, $\mathbf{v}_{,\alpha}$ and $-\mathbf{v}_{,\alpha}|_\beta$, in strains $\varepsilon_{\alpha\beta}$, $\kappa_{\alpha\beta}$ are
²²⁵ approximated by $(p-1)$ -th order polynomials in each integration cells. In inte-
²²⁶ gration cell Ω_C , the approximated derivatives and strains denoted by $\mathbf{v}_{,\alpha}^h$, $\varepsilon_{\alpha\beta}^h$
²²⁷ and $-\mathbf{v}_{,\alpha}^h|_\beta$, $\kappa_{\alpha\beta}^h$ can be expressed by:

$$\mathbf{v}_{,\alpha}^h(\boldsymbol{\xi}) = \mathbf{q}^T(\boldsymbol{\xi}) \mathbf{d}_\alpha^\varepsilon, \quad \varepsilon_{\alpha\beta}^h(\boldsymbol{\xi}) = \mathbf{q}^T(\boldsymbol{\xi}) \frac{1}{2} (\mathbf{a}_\alpha \cdot \mathbf{d}_\beta^\varepsilon + \mathbf{a}_\beta \cdot \mathbf{d}_\alpha^\varepsilon) \quad (32)$$

$$-\mathbf{v}_{,\alpha}^h|_\beta(\boldsymbol{\xi}) = \mathbf{q}^T(\boldsymbol{\xi}) \mathbf{d}_{\alpha\beta}^\kappa, \quad \kappa_{\alpha\beta}^h(\boldsymbol{\xi}) = \mathbf{q}^T(\boldsymbol{\xi}) \mathbf{a}_3 \cdot \mathbf{d}_{\alpha\beta}^\kappa \quad (33)$$

²²⁸ where \mathbf{q} is the linear polynomial vector and has the following form:

$$\mathbf{q} = \{1, \xi^1, \xi^2\}^T \quad (34)$$

²³⁰ and the $\mathbf{d}_\alpha^\varepsilon$, $\mathbf{d}_{\alpha\beta}^\kappa$ are the corresponding coefficient vector tensors. For the con-
²³¹ ciseness, the mixed usage of tensor and vector is introduced in this study. For
²³² instance, the component of coefficient tensor vector $\mathbf{d}_{\alpha I}^\varepsilon$, $\mathbf{d}_\alpha^\varepsilon = \{\mathbf{d}_{\alpha I}^\varepsilon\}$, is a three
²³³ dimensional tensor, $\dim \mathbf{d}_{\alpha I}^\varepsilon = \dim \mathbf{v}$.

²³⁴ To satisfy the integration constraint of thin shell problem, the approximated
²³⁵ stresses $N^{\alpha\beta h}$, $M^{\alpha\beta h}$ were assumed to have a comparable form to strains, and
²³⁶ yields:

$$N^{\alpha\beta h}(\boldsymbol{\xi}) = \mathbf{q}^T(\boldsymbol{\xi}) \mathbf{a}^\alpha \cdot \mathbf{d}_N^\beta, \quad \mathbf{a}_\alpha N^{\alpha\beta h}(\boldsymbol{\xi}) = \mathbf{q}^T(\boldsymbol{\xi}) \mathbf{d}_N^\beta \quad (35)$$

$$M^{\alpha\beta h}(\boldsymbol{\xi}) = \mathbf{q}^T(\boldsymbol{\xi}) \mathbf{a}_3 \cdot \mathbf{d}_M^{\alpha\beta}, \quad \mathbf{a}_3 M^{\alpha\beta h}(\boldsymbol{\xi}) = \mathbf{q}^T(\boldsymbol{\xi}) \mathbf{d}_M^{\alpha\beta} \quad (36)$$

²³⁷ substituting the approximations of Eqs. (22), (32), (33), (35), (36) into Eqs.
²³⁸ (21c), (21d) can express $\mathbf{d}_\beta^\varepsilon$ and $\mathbf{d}_{\alpha\beta}^\kappa$ by \mathbf{d} as:

$$\mathbf{d}_\beta^\varepsilon = \mathbf{G}^{-1} \left(\sum_{I=1}^{n_p} (\tilde{\mathbf{g}}_{\beta I} - \bar{\mathbf{g}}_{\beta I}) \mathbf{d}_I + \hat{\mathbf{g}}_\beta \right) \quad (37)$$

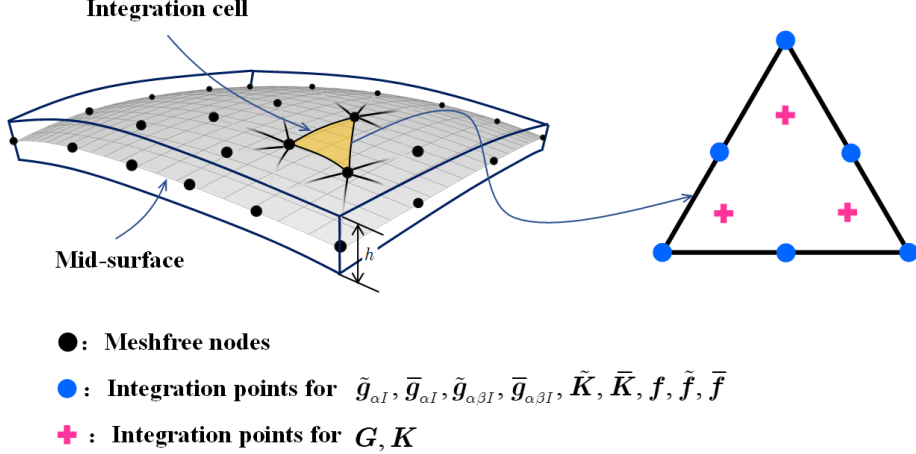


Figure 2: Integration scheme for Hu-Washizu weak form.

240

$$\mathbf{d}_{\alpha\beta}^\kappa = \mathbf{G}^{-1} \left(\sum_{I=1}^{n_p} (\tilde{\mathbf{g}}_{\alpha\beta I} - \bar{\mathbf{g}}_{\alpha\beta I}) \mathbf{d}_I + \hat{\mathbf{g}}_{\alpha\beta} \right) \quad (38)$$

241 with

$$\mathbf{G} = \int_{\Omega_C} \mathbf{q}^T \mathbf{q} d\Omega \quad (39)$$

242

$$\tilde{\mathbf{g}}_{\beta I} = \int_{\Gamma_C} \Psi_I \mathbf{q} n_\beta d\Gamma - \int_{\Omega_C} \Psi_I \mathbf{q}_{|\beta} d\Omega \quad (40a)$$

$$\bar{\mathbf{g}}_{\beta I} = \int_{\Gamma_C \cap \Gamma_v} \Psi_I \mathbf{q} n_\beta d\Gamma \quad (40b)$$

$$\hat{\mathbf{g}}_\beta = \int_{\Gamma_C \cap \Gamma_v} \mathbf{q} n_\beta \bar{\mathbf{v}} d\Gamma \quad (40c)$$

243

$$\begin{aligned} \tilde{\mathbf{g}}_{\alpha\beta I} &= \int_{\Gamma_C} \Psi_{I,\gamma} n^\gamma \mathbf{q} n_\alpha n_\beta d\Gamma - \int_{\Gamma_C} \Psi_I (\mathbf{q}_{|\beta} n_\alpha + (\mathbf{q} s_\alpha n_\beta)_{,\gamma} s^\gamma) d\Gamma \\ &\quad + [[\Psi_I \mathbf{q} s_\alpha n_\beta]]_{\mathbf{x} \in C_C} - \int_{\Omega_C} \Psi_I \mathbf{q}_{,\alpha|\beta} d\Omega \end{aligned} \quad (41a)$$

$$\begin{aligned} \bar{\mathbf{g}}_{\alpha\beta I} &= \int_{\Gamma_C \cap \Gamma_\theta} \Psi_{I,\gamma} n^\gamma \mathbf{q} n_\alpha n_\beta d\Gamma - \int_{\Gamma_C \cap \Gamma_v} \Psi_I (\mathbf{q}_{|\beta} n_\alpha + (\mathbf{q} s_\alpha n_\beta)_{,\gamma} s^\gamma) d\Gamma \\ &\quad + [[\Psi_I \mathbf{q} s_\alpha n_\beta]]_{\mathbf{x} \in C_C \cap C_v} \end{aligned} \quad (41b)$$

$$\begin{aligned} \hat{\mathbf{g}}_{\alpha\beta} &= \int_{\Gamma_C \cap \Gamma_\theta} \mathbf{q} n_\alpha n_\beta \bar{\mathbf{a}}_3 \bar{\mathbf{n}} d\Gamma - \int_{\Gamma_C \cap \Gamma_v} (\mathbf{q}_{|\beta} n_\alpha + (\mathbf{q} s_\alpha n_\beta)_{,\gamma} s^\gamma) \bar{\mathbf{v}} d\Gamma \\ &\quad + [[\mathbf{q} s_\alpha n_\beta \bar{\mathbf{v}}]]_{\mathbf{x} \in C_C \cap C_v} \end{aligned} \quad (41c)$$

²⁴⁴ where the derivations of $\mathbf{q}_{|\beta}$, $\mathbf{q}_{,\alpha|\beta}$ are discussed in detail in Appendix A. Further
²⁴⁵ plugging Eqs. (37) and (38) back into Eqs. (32) and (33), respectively gives the
²⁴⁶ final expression of $\mathbf{v}_{,\alpha}^h$, $\varepsilon_{\alpha\beta}^h$ and $-\mathbf{v}_{,\alpha\beta}^h$, $\kappa_{\alpha\beta}^h$ as:

$$\mathbf{v}_{,\alpha}^h = \sum_{I=1}^{n_p} (\tilde{\Psi}_{I,\alpha} - \bar{\Psi}_{I,\alpha}) \mathbf{d}_I + \mathbf{q}^T \mathbf{G}^{-1} \hat{\mathbf{g}}_\alpha \quad (42a)$$

$$\begin{aligned} \varepsilon_{\alpha\beta}^h &= \sum_{I=1}^{n_p} \frac{1}{2} (\mathbf{a}_\alpha \tilde{\Psi}_{I,\beta} + \mathbf{a}_\beta \tilde{\Psi}_{I,\alpha}) \cdot \mathbf{d}_I - \sum_{I=1}^{n_p} \frac{1}{2} (\mathbf{a}_\alpha \bar{\Psi}_{I,\beta} + \mathbf{a}_\beta \bar{\Psi}_{I,\alpha}) \cdot \mathbf{d}_I \\ &\quad + \mathbf{q}^T \mathbf{G}^{-1} \frac{1}{2} (\mathbf{a}_\alpha \cdot \hat{\mathbf{g}}_\beta + \mathbf{a}_\beta \cdot \hat{\mathbf{g}}_\alpha) \\ &= \tilde{\varepsilon}_{\alpha\beta}^h - \bar{\varepsilon}_{\alpha\beta}^h + \hat{\varepsilon}_{\alpha\beta}^h \end{aligned} \quad (42b)$$

²⁴⁸

$$-\mathbf{v}_{,\alpha}^h|_\beta = \sum_{I=1}^{n_p} (\tilde{\Psi}_{I,\alpha\beta} - \bar{\Psi}_{I,\alpha\beta}) \mathbf{d}_I + \mathbf{q}^T \mathbf{G}^{-1} \hat{\mathbf{g}}_{\alpha\beta} \quad (43a)$$

²⁴⁹

$$\begin{aligned} \kappa_{\alpha\beta}^h &= \sum_{I=1}^{n_p} \tilde{\Psi}_{I,\alpha\beta} \mathbf{a}_3 \cdot \mathbf{d}_I - \sum_{I=1}^{n_p} \bar{\Psi}_{I,\alpha\beta} \mathbf{a}_3 \cdot \mathbf{d}_I + \mathbf{q}^T \mathbf{G}^{-1} \mathbf{a}_3 \cdot \hat{\mathbf{g}}_{\alpha\beta} \\ &= \tilde{\kappa}_{\alpha\beta}^h - \bar{\kappa}_{\alpha\beta}^h + \hat{\kappa}_{\alpha\beta}^h \end{aligned} \quad (43b)$$

²⁵⁰ with

$$\begin{cases} \tilde{\varepsilon}_{\alpha\beta}^h = \sum_{I=1}^{n_p} \frac{1}{2} (\mathbf{a}_\alpha \tilde{\Psi}_{I,\beta} + \mathbf{a}_\beta \tilde{\Psi}_{I,\alpha}) \cdot \mathbf{d}_I = \sum_{I=1}^{n_p} \tilde{\varepsilon}_{\alpha\beta I} \cdot \mathbf{d}_I \\ \bar{\varepsilon}_{\alpha\beta}^h = \sum_{I=1}^{n_p} \frac{1}{2} (\mathbf{a}_\alpha \bar{\Psi}_{I,\beta} + \mathbf{a}_\beta \bar{\Psi}_{I,\alpha}) \cdot \mathbf{d}_I = \sum_{I=1}^{n_p} \bar{\varepsilon}_{\alpha\beta I} \cdot \mathbf{d}_I \\ \hat{\varepsilon}_{\alpha\beta}^h = \mathbf{q}^T \mathbf{G}^{-1} \frac{1}{2} (\mathbf{a}_\alpha \cdot \hat{\mathbf{g}}_\beta + \mathbf{a}_\beta \cdot \hat{\mathbf{g}}_\alpha) \end{cases} \quad (44)$$

²⁵¹

$$\begin{cases} \tilde{\Psi}_{I,\alpha}(\boldsymbol{\xi}) = \mathbf{q}^T(\boldsymbol{\xi}) \mathbf{G}^{-1} \tilde{\mathbf{g}}_{\alpha I} \\ \bar{\Psi}_{I,\alpha}(\boldsymbol{\xi}) = \mathbf{q}^T(\boldsymbol{\xi}) \mathbf{G}^{-1} \bar{\mathbf{g}}_{\alpha I} \\ \tilde{\varepsilon}_{\alpha\beta I} = \frac{1}{2} (\mathbf{a}_\alpha \tilde{\Psi}_{I,\beta} + \mathbf{a}_\beta \tilde{\Psi}_{I,\alpha}) \\ \bar{\varepsilon}_{\alpha\beta I} = \frac{1}{2} (\mathbf{a}_\alpha \bar{\Psi}_{I,\beta} + \mathbf{a}_\beta \bar{\Psi}_{I,\alpha}) \end{cases} \quad (45)$$

²⁵²

$$\begin{cases} \tilde{\kappa}_{\alpha\beta}^h = \sum_{I=1}^{n_p} \tilde{\Psi}_{I,\alpha\beta} \mathbf{a}_3 \cdot \mathbf{d}_I = \sum_{I=1}^{n_p} \tilde{\kappa}_{\alpha\beta I} \cdot \mathbf{d}_I \\ \bar{\kappa}_{\alpha\beta}^h = \sum_{I=1}^{n_p} \bar{\Psi}_{I,\alpha\beta} \mathbf{a}_3 \cdot \mathbf{d}_I = \sum_{I=1}^{n_p} \bar{\kappa}_{\alpha\beta I} \cdot \mathbf{d}_I \\ \hat{\kappa}_{\alpha\beta}^h = \mathbf{q}^T \mathbf{G}^{-1} \mathbf{a}_3 \cdot \hat{\mathbf{g}}_{\alpha\beta} \end{cases} \quad (46)$$

253

$$\begin{cases} \tilde{\Psi}_{I,\alpha\beta}(\xi) = \mathbf{q}^T(\xi) \mathbf{G}^{-1} \tilde{\mathbf{g}}_{\alpha\beta I} \\ \bar{\Psi}_{I,\alpha\beta}(\xi) = \mathbf{q}^T(\xi) \mathbf{G}^{-1} \tilde{\mathbf{g}}_{\alpha\beta I} \\ \tilde{\kappa}_{\alpha\beta I} = \tilde{\Psi}_{I,\alpha\beta} \mathbf{a}_3 \\ \bar{\kappa}_{\alpha\beta I} = \bar{\Psi}_{I,\alpha\beta} \mathbf{a}_3 \end{cases} \quad (47)$$

254 It has to be noted that, referring to reproducing kernel gradient smoothing
 255 framework [26], $\tilde{\Psi}_{I,\alpha}$, $\tilde{\Psi}_{I,\alpha\beta}$ are actually the first and second order smoothed
 256 gradients in curvilinear coordinates. If the right hand side integration constraints
 257 for first and second order gradients are $\tilde{\mathbf{g}}_{\alpha I}$ and $\tilde{\mathbf{g}}_{\alpha\beta I}$, respectively, then this for-
 258 mulation can satisfy the variational consistency for the second order polynomi-
 259 als. It should be mentioned that in curved model, the variational consistency for
 260 non-polynomial functions, such as trigonometric functions, should be required
 261 for the polynomial solution. Even with high order polynomial variational consis-
 262 tency, the proposed formulation cannot exactly reproduce the solution spanned
 263 by the basis functions. However, the accuracy of reproducing kernel smoothed
 264 gradients is still superior than the traditional meshfree formulation. The numer-
 265 ical examples in the following section will better demonstrate to the precision
 266 of the reproducing kernel smoothed gradients.

²⁶⁷ **4. Naturally variational enforcement for essential boundary condi-**
²⁶⁸ **tions**

²⁶⁹ *4.1. Discrete equilibrium equations*

²⁷⁰ With the approximated effective stresses and strains, the last equation of
²⁷¹ weak form Eq. (21e) becomes:

$$-\sum_{C=1}^{n_e} \sum_{I=1}^{n_p} \delta \mathbf{d}_I \cdot \left((\tilde{\mathbf{g}}_{\alpha I}^T - \bar{\mathbf{g}}_{\alpha I}^T) \mathbf{d}_N^\alpha + (\tilde{\mathbf{g}}_{\alpha\beta I}^T - \bar{\mathbf{g}}_{\alpha\beta I}^T) \mathbf{d}_M^{\alpha\beta} \right) = -\sum_{I=1}^{n_p} \delta d_I \cdot \mathbf{f}_I \quad (48)$$

²⁷² where \mathbf{f}_I 's denote the components of the traditional force vector:

$$\mathbf{f}_I = \int_{\Gamma_t} \Psi_I \bar{\mathbf{t}} d\Gamma - \int_{\Gamma_M} \Psi_{I,\gamma} n^\gamma \bar{M}_{\mathbf{n}\mathbf{n}} d\Gamma + [[\Psi_I \mathbf{a}_3 \bar{P}]]_{\mathbf{x} \in C_P} + \int_{\Omega} \Psi_I \bar{\mathbf{b}} d\Omega \quad (49)$$

²⁷³ The left side of Eq. (48) can be simplified using the following steps. For clarity,
²⁷⁴ the derivation of first term in Eq. (48) taken as an example is given by:

$$\begin{aligned} \sum_{I=1}^{n_p} \delta \mathbf{d}_I \cdot \tilde{\mathbf{g}}_{\alpha I}^T \mathbf{d}_N^\alpha &= \sum_{I=1}^{n_p} \delta \mathbf{d}_I \cdot (\mathbf{G}^{-1} \tilde{\mathbf{g}}_{\alpha I})^T \mathbf{G} \mathbf{d}_N^\alpha \\ &= \int_{\Omega_C} \sum_{I=1}^{n_p} \delta \mathbf{d}_I \cdot (\mathbf{q}^T \mathbf{G}^{-1} \tilde{\mathbf{g}}_{\alpha I})^T \mathbf{q}^T \mathbf{d}_N^\alpha d\Omega \\ &= \int_{\Omega_C} \sum_{I=1}^{n_p} \delta \mathbf{d}_I \cdot \mathbf{a}_\beta (\mathbf{q}^T \mathbf{G}^{-1} \tilde{\mathbf{g}}_{\alpha I})^T N^{\alpha\beta h} d\Omega \\ &= \int_{\Omega_C} \delta \hat{\varepsilon}_{\alpha\beta}^h N^{\alpha\beta h} d\Omega \end{aligned} \quad (50)$$

²⁷⁵ following the above procedure and including the weak form of Eqs. (21a), (21b),
²⁷⁶ the left side of Eq. (48) in Ω_C becomes:

$$\begin{aligned}
& \sum_{I=1}^{n_p} \delta \mathbf{d}_I \cdot \left((\tilde{\mathbf{g}}_{\alpha I}^T - \bar{\mathbf{g}}_{\alpha I}^T) \mathbf{d}_N^\alpha + (\tilde{\mathbf{g}}_{\alpha \beta I}^T - \bar{\mathbf{g}}_{\alpha \beta I}^T) \mathbf{d}_M^{\alpha \beta} \right) \\
& = \int_{\Omega_C} ((\delta \tilde{\varepsilon}_{\alpha \beta}^h - \delta \bar{\varepsilon}_{\alpha \beta}^h) N^{\alpha \beta h} + (\delta \tilde{\kappa}_{\alpha \beta}^h - \delta \bar{\kappa}_{\alpha \beta}^h) M^{\alpha \beta h}) d\Omega \\
& = \int_{\Omega_C} (\delta \tilde{\varepsilon}_{\alpha \beta}^h - \delta \bar{\varepsilon}_{\alpha \beta}^h) h C^{\alpha \beta \gamma \eta} \varepsilon_{\gamma \eta}^h + (\delta \tilde{\kappa}_{\alpha \beta}^h - \delta \bar{\kappa}_{\alpha \beta}^h) \frac{h^3}{12} C^{\alpha \beta \gamma \eta} \kappa_{\gamma \eta}^h \\
& = \int_{\Omega_C} \delta \tilde{\varepsilon}_{\alpha \beta}^h h C^{\alpha \beta \gamma \eta} \tilde{\varepsilon}_{\gamma \eta}^h d\Omega + \int_{\Omega_C} \delta \tilde{\kappa}_{\alpha \beta}^h \frac{h^3}{12} C^{\alpha \beta \gamma \eta} \tilde{\kappa}_{\gamma \eta}^h d\Omega \\
& - \int_{\Omega_C} \delta \tilde{\varepsilon}_{\alpha \beta}^h h C^{\alpha \beta \gamma \eta} \bar{\varepsilon}_{\gamma \eta}^h d\Omega - \int_{\Omega_C} \delta \bar{\varepsilon}_{\alpha \beta}^h h C^{\alpha \beta \gamma \eta} \tilde{\varepsilon}_{\gamma \eta}^h d\Omega \\
& - \int_{\Omega_C} \delta \tilde{\kappa}_{\alpha \beta}^h \frac{h^3}{12} C^{\alpha \beta \gamma \eta} \bar{\kappa}_{\gamma \eta}^h d\Omega - \int_{\Omega_C} \delta \bar{\kappa}_{\alpha \beta}^h \frac{h^3}{12} C^{\alpha \beta \gamma \eta} \tilde{\kappa}_{\gamma \eta}^h d\Omega \\
& + \int_{\Omega_C} \delta \bar{\varepsilon}_{\alpha \beta}^h h C^{\alpha \beta \gamma \eta} \tilde{\varepsilon}_{\gamma \eta}^h d\Omega + \int_{\Omega_C} \delta \bar{\kappa}_{\alpha \beta}^h \frac{h^3}{12} C^{\alpha \beta \gamma \eta} \bar{\kappa}_{\gamma \eta}^h d\Omega \\
& + \int_{\Omega_C} (\delta \tilde{\varepsilon}_{\alpha \beta}^h - \delta \bar{\varepsilon}_{\alpha \beta}^h) h C^{\alpha \beta \gamma \eta} \hat{\varepsilon}_{\gamma \eta}^h d\Omega + \int_{\Omega_C} (\delta \tilde{\kappa}_{\alpha \beta}^h - \delta \bar{\kappa}_{\alpha \beta}^h) \frac{h^3}{12} C^{\alpha \beta \gamma \eta} \hat{\kappa}_{\gamma \eta}^h d\Omega
\end{aligned} \tag{51}$$

²⁷⁷ The complete discrete equilibrium equations can be obtained by further substituting Eqs. (44) and (46) into above equation, respectively:
²⁷⁸

$$(\mathbf{K} + \tilde{\mathbf{K}} + \bar{\mathbf{K}}) \mathbf{d} = \mathbf{f} + \tilde{\mathbf{f}} + \bar{\mathbf{f}} \tag{52}$$

²⁷⁹ where

$$\mathbf{K}_{IJ} = \int_{\Omega} \tilde{\varepsilon}_{\alpha \beta I} h C^{\alpha \beta \gamma \eta} \tilde{\varepsilon}_{\gamma \eta J} d\Omega + \int_{\Omega} \tilde{\kappa}_{\alpha \beta I} \frac{h^3}{12} C^{\alpha \beta \gamma \eta} \tilde{\kappa}_{\alpha \beta J} d\Omega \tag{53}$$

²⁸⁰

$$\begin{aligned}
\tilde{\mathbf{K}}_{IJ} = & - \int_{\Gamma_v} (\Psi_I \tilde{\mathbf{T}}_{NJ} + \tilde{\mathbf{T}}_{NJ} \Psi_J) d\Gamma \\
& + \int_{\Gamma_\theta} (\Psi_{I,\gamma} n^\gamma \mathbf{a}_3 \tilde{\mathbf{M}}_{nnJ} + \mathbf{a}_3 \tilde{\mathbf{M}}_{nnI} \Psi_{I,\gamma} n^\gamma) d\Gamma \\
& + ([[\Psi_I \mathbf{a}_3 \tilde{\mathbf{P}}_J]] + [[\tilde{\mathbf{P}}_I \mathbf{a}_3 \Psi_J]])_{\mathbf{x} \in C_v}
\end{aligned} \tag{54a}$$

$$\tilde{\mathbf{f}}_I = - \int_{\Gamma_v} \tilde{\mathbf{T}}_{NI} \cdot \bar{\mathbf{v}} d\Gamma + \int_{\Gamma_\theta} \tilde{\mathbf{M}}_{nnI} \bar{\theta}_n d\Gamma + [[\tilde{\mathbf{P}}_I \mathbf{a}_3 \cdot \bar{\mathbf{v}}]]_{\mathbf{x} \in C_v} \tag{54b}$$

²⁸¹

$$\bar{\mathbf{K}}_{IJ} = - \int_{\Gamma_v} \bar{\mathbf{T}}_{MI} \Psi_J d\Gamma + \int_{\Gamma_\theta} \mathbf{a}_3 \bar{\mathbf{M}}_{nnI} \Psi_{J,\gamma} n^\gamma d\Gamma + [[\bar{\mathbf{P}}_I \mathbf{a}_3 \Psi_J]]_{\mathbf{x} \in C_v} \tag{55a}$$

$$\bar{\mathbf{f}}_I = - \int_{\Gamma_v} \bar{\mathbf{T}}_{MI} \cdot \bar{\mathbf{v}} d\Gamma + \int_{\Gamma_\theta} \bar{\mathbf{M}}_{nnI} \bar{\theta}_n d\Gamma + [[\bar{\mathbf{P}}_I \mathbf{a}_3 \cdot \bar{\mathbf{v}}]]_{\mathbf{x} \in C_v} \tag{55b}$$

282 The detailed derivations of Eqs (53)-(55) are listed in the Appendix B. As
 283 shown in these equations, Eq. (53) is the conventional stiffness matrix eval-
 284 uated by smoothed gradients $\tilde{\Psi}_{I,\alpha}$, $\tilde{\Psi}_{I,\alpha}|_{\beta}$, and the Eqs. (54) and (55) contribute
 285 for the enforcement of essential boundary. It should be noticed that, in accor-
 286 dance with reproducing kernel smoothed gradient framework, the integration
 287 scheme of Eqs. (53-55) should be aligned with those used in the construction of
 288 smoothed gradients. The integration scheme used for the proposed method is
 289 shown in Fig. 2, in which the total number of the blue circular integration points
 290 has been optimized from a global point of view, aiming to reduce the computa-
 291 tion of traditional meshfree shape functions and its first order derivatives. In
 292 contrast, for assembly stiffness matrix \mathbf{K} , the low order Gauss integration rule
 293 is suitable to ensure the accuracy due to the inherently variational consistency
 294 in the smoothed gradients. The detailed positions and weight of the integration
 295 points and the efficiency demonstration of this optimized integration scheme
 296 can be found in [26, 32]. Examining Eqs. (54) and (55), closely reveal that the
 297 structure of the suggested approach to enforce essential boundary conditions is
 298 identical to that of the conventional Nitsche’s method, with both having the
 299 consistent and stabilized terms. Thus, a review of Nitsche’s method and a com-
 300 parison with the proposed approach will be provided in the next subsection.

301 *4.2. Comparison with Nitsche’s method*

302 The Nitsche’s method for enforcing essential boundaries can be regarded as a
 303 combination of Lagrangian multiplier method and penalty method, in which the
 304 Lagrangian multiplier is represented by the approximated displacement. The
 305 corresponding total potential energy functional Π_P is given by:

$$\begin{aligned}
 \Pi_P(\mathbf{v}) = & \int_{\Omega} \frac{1}{2} \varepsilon_{\alpha\beta} N^{\alpha\beta} d\Omega + \int_{\Omega} \frac{1}{2} \kappa_{\alpha\beta} M^{\alpha\beta} d\Omega \\
 & - \int_{\Gamma_t} \mathbf{v} \cdot \bar{\mathbf{t}} d\Gamma + \int_{\Gamma_M} \mathbf{v}_{,\gamma} n^{\gamma} \mathbf{a}_3 M_{\mathbf{n}\mathbf{n}} d\Gamma + (\mathbf{v} \cdot \mathbf{a}_3 P)_{\mathbf{x} \in C_P} - \int_{\Omega} \mathbf{v} \cdot \bar{\mathbf{b}} d\Omega \\
 & - \underbrace{\int_{\Gamma_v} \mathbf{t} \cdot (\mathbf{v} - \bar{\mathbf{v}}) d\Gamma + \int_{\Gamma_{\theta}} M_{\mathbf{n}\mathbf{n}} (\theta_{\mathbf{n}} - \bar{\theta}_{\mathbf{n}}) d\Gamma + (P \mathbf{a}_3 \cdot (\mathbf{v} - \bar{\mathbf{v}}))_{\mathbf{x} \in C_v}}_{\text{consistent term}} \\
 & + \underbrace{\sum_{i=1}^3 \frac{\alpha_{vi}}{2} \int_{\Gamma_v} \mathbf{v} \cdot \mathbf{v} d\Gamma + \frac{\alpha_{\theta}}{2} \int_{\Gamma_{\theta}} \theta_{\mathbf{n}}^2 d\Gamma + \frac{\alpha_C}{2} (\mathbf{v} \cdot \mathbf{a}_3)_{\mathbf{x} \in C_v}^2}_{\text{stabilized term}}
 \end{aligned} \quad (56)$$

306 where the consistent term generated from the Lagrangian multiplier method con-
 307 tributes to enforce the essential boundary, and meet the variational consistency
 308 condition. However, the consistent term cannot always ensure the coercivity of
 309 stiffness, so the penalty method is introduced to serve as a stabilized term, in
 310 which α_{vi} ’s, α_{θ} and α_C are experimental artificial parameters in the penalty
 311 method. With a standard variational argument, the corresponding weak form

³¹² can be stated as:

$$\begin{aligned}
\delta\Pi_P(\mathbf{v}) &= \int_{\Omega} \delta\varepsilon_{\alpha\beta} N^{\alpha\beta} d\Omega + \int_{\Omega} \delta\kappa_{\alpha\beta} M^{\alpha\beta} d\Omega \\
&\quad - \int_{\Gamma_t} \delta\mathbf{v} \cdot \bar{\mathbf{t}} d\Gamma + \int_{\Gamma_M} \delta\mathbf{v}_{,\gamma} n^\gamma \mathbf{a}_3 M_{\mathbf{n}\mathbf{n}} d\Gamma + (\delta\mathbf{v} \cdot \mathbf{a}_3 P)_{\mathbf{x} \in C_P} - \int_{\Omega} \delta\mathbf{v} \cdot \bar{\mathbf{b}} d\Omega \\
&\quad - \int_{\Gamma_v} \delta\mathbf{v} \cdot \mathbf{t} d\Gamma + \int_{\Gamma_\theta} \delta\theta_{\mathbf{n}} M_{\mathbf{n}\mathbf{n}} d\Gamma + (\mathbf{v} \cdot \mathbf{a}_3 P)_{\mathbf{x} \in C_v} \\
&\quad - \int_{\Gamma_v} \delta\mathbf{t} \cdot (\mathbf{v} - \bar{\mathbf{v}}) d\Gamma + \int_{\Gamma_\theta} \delta M_{\mathbf{n}\mathbf{n}} (\theta_{\mathbf{n}} - \bar{\theta}_{\mathbf{n}}) d\Gamma + (\delta P \mathbf{a}_3 \cdot (\mathbf{v} - \bar{\mathbf{v}}))_{\mathbf{x} \in C_v} \\
&\quad + \sum_{i=1}^3 \alpha_{vi} \int_{\Gamma_v} (\delta\mathbf{v} \cdot \mathbf{a}_i) (\mathbf{a}_i \cdot \mathbf{v}) d\Gamma + \alpha_\theta \int_{\Gamma_\theta} \delta\theta_{\mathbf{n}} \theta_{\mathbf{n}} d\Gamma + \alpha_C (\delta\mathbf{v} \cdot \mathbf{a}_3 \mathbf{a}_3 \cdot \mathbf{v})_{\mathbf{x} \in C_v} \\
&= 0
\end{aligned} \tag{57}$$

³¹³ Upon further invoking the conventional reproducing kernel approximation of
³¹⁴ Eq. (22), the subsequent discrete equilibrium equations can be obtained:

$$\sum_{J=1}^{n_p} (\mathbf{K}_{IJ} + \mathbf{K}_{IJ}^c + \mathbf{K}_{IJ}^s) \mathbf{d}_J = \mathbf{f}_I + \mathbf{f}^c + \mathbf{f}^s \tag{58}$$

³¹⁵ where the stiffness \mathbf{K}_{IJ} is identical with Eq. (53). \mathbf{K}_{IJ}^c and \mathbf{K}_{IJ}^s are the stiffness
³¹⁶ matrices for consistent and stabilized terms, respectively, and have the following
³¹⁷ form:

$$\begin{aligned}
\mathbf{K}_{IJ}^c &= - \int_{\Gamma_v} (\Psi_I \mathbf{T}_{NJ} + \mathbf{T}_{NJ} \Psi_J) d\Gamma \\
&\quad + \int_{\Gamma_\theta} (\Psi_{I,\gamma} n^\gamma \mathbf{a}_3 M_{\mathbf{n}\mathbf{n},J} + \mathbf{a}_3 M_{\mathbf{n}\mathbf{n},I} \Psi_{I,\gamma} n^\gamma) d\Gamma \\
&\quad + ([[\Psi_I \mathbf{a}_3 \mathbf{P}_J]] + [[\mathbf{P}_I \mathbf{a}_3 \Psi_J]])_{\mathbf{x} \in C_v}
\end{aligned} \tag{59a}$$

$$\mathbf{f}_I^c = - \int_{\Gamma_v} \mathbf{T}_I \cdot \bar{\mathbf{v}} d\Gamma + \int_{\Gamma_\theta} \mathbf{M}_{\mathbf{n}\mathbf{n},I} \bar{\theta}_{\mathbf{n}} d\Gamma + [[\mathbf{P}_I \mathbf{a}_3 \cdot \bar{\mathbf{v}}]]_{\mathbf{x} \in C_v} \tag{59b}$$

³¹⁸

$$\mathbf{K}_{IJ}^s = \boldsymbol{\alpha}_v \int_{\Gamma_v} \Psi_I \Psi_J d\Gamma + \alpha_\theta \int_{\Gamma_\theta} \Psi_{I,\eta} n^\eta \mathbf{a}_3 \mathbf{a}_3 n^\gamma \Psi_{J,\gamma} d\Gamma + \alpha_C [[\Psi_I \mathbf{a}_3 \mathbf{a}_3 \Psi_J]]_{\mathbf{x} \in C_v} \tag{60a}$$

$$\mathbf{f}_I^s = \boldsymbol{\alpha}_v \int_{\Gamma_v} \Psi_I \bar{\mathbf{v}} d\Gamma + \alpha_\theta \int_{\Gamma_\theta} \Psi_{I,\eta} n^\eta \mathbf{a}_3 \bar{\theta}_{\mathbf{n}} d\Gamma + \alpha_C [[\Psi_I \mathbf{a}_3 \mathbf{a}_3 \cdot \bar{\mathbf{v}}]]_{\mathbf{x} \in C_v} \tag{60b}$$

³¹⁹ with

$$\boldsymbol{\alpha}_v = \begin{bmatrix} \alpha_{v1} & 0 & 0 \\ 0 & \alpha_{v2} & 0 \\ 0 & 0 & \alpha_{v3} \end{bmatrix} \tag{61}$$

320 On comparing with the consistent terms of Eqs. (54) and (59), the ex-
321 pressions were almost identical, the major difference is that the higher order
322 derivatives of shape functions have been replaced by the smoothed gradients.
323 Owing to the reproducing kernel framework, the construction of the smoothed
324 gradients only concerned about the computation of traditional meshfree shape
325 functions and their first order derivatives, which avoid the costly computation
326 of higher order derivatives. Moreover, the stabilized terms in Eq. (60) em-
327 ploys the penalty method with big enough artificial parameters to ensure the
328 coercivity of stiffness. Besides, the optimal values of these artificial parame-
329 ters are proportional to the grid size of discrete model that can be represented
330 by the support size in meshfree approximation, where $\alpha_{v\alpha} \propto s^{-1}$, $\alpha_{v3} \propto s^{-3}$,
331 $\alpha_\theta \propto s^{-1}$, $\alpha_C \propto s^{-2}$ [30], and $s = \min\{s_{\alpha I}\}$. In contrast, the stabilized term of
332 Eq. (55) naturally exists in its weak form, and can stabilize the result without
333 considering any artificial parameters.

334 **5. Numerical examples**

335 In this section, the suggested method is validated through several exam-
 336 ples using the Nitsche's method, the consistent reproducing kernel gradient
 337 smoothing integration scheme (RKGSI), and the non-consistent Gauss integra-
 338 tion scheme (GI) with penalty method, as well as the proposed Hu-Washizu
 339 formulation (HW) to enforce the necessary boundary conditions. A normalized
 340 support size of 2.5 is used for all the considered methods to ensure the require-
 341 ment of quadratic base meshfree approximation. To eliminate the influence of
 342 integration error, the Gauss integration scheme uses 6 Gauss points for domain
 343 integration and 3 points for boundary integration, so as to maintain the same
 344 integration accuracy between domain and boundaries. Moreover, the number
 345 of integration points are identical between the Gauss and RKGSI schemes. The
 346 error estimates of displacement (L_2 -Error) and energy (H_e -Error) is used here:

$$L_2\text{-Error} = \frac{\sqrt{\int_{\Omega}(\mathbf{v} - \mathbf{v}^h) \cdot (\mathbf{v} - \mathbf{v}^h) d\Omega}}{\sqrt{\mathbf{v} \cdot \mathbf{v}}}$$

$$H_e\text{-Error} = \frac{\sqrt{\int_{\Omega} ((\varepsilon_{\alpha\beta} - \varepsilon_{\alpha\beta}^h)(N^{\alpha\beta} - N^{\alpha\beta h}) + \int_{\Omega} (\kappa_{\alpha\beta} - \kappa_{\alpha\beta}^h)(M^{\alpha\beta} - M^{\alpha\beta h})) d\Omega}}{\sqrt{\int_{\Omega} (\varepsilon_{\alpha\beta} N^{\alpha\beta} + \kappa_{\alpha\beta} M^{\alpha\beta}) d\Omega}}$$
(62)

347 *5.1. Patch tests*

348 The linear and quadratic patch tests for flat and curved thin shells are firstly
 349 studied to verify the variational consistency of the proposed method. As shown
 350 in Fig. 3, the flat and curved models are depicted by an identical parametric
 351 domain $\Omega = (0, 1) \otimes (0, 1)$, where the cylindrical coordinate system with radius
 352 $R = 1$ is employed to describe the curved model, and the whole domain Ω
 353 is discretized by the 165 meshfree nodes. The artificial parameters of $\alpha_v =$
 354 10^5 , $\alpha_\theta = 10^3$, $\alpha_C = 10^5$ and $\alpha_v = 10^9$, $\alpha_\theta = 10^9$, $\alpha_C = 10^9$ were adopted in
 355 Nitsche's- and penalty- method, respectively. All the boundaries are enforced
 356 as essential boundary conditions with the following manufactured exact solution:

$$\mathbf{v} = \begin{cases} (\xi^1 + 2\xi^2)^n \\ (3\xi^1 + 4\xi^2)^n \\ (5\xi^1 + 6\xi^2)^n \end{cases}, \quad n = \begin{cases} 1 & \text{Linear patch test} \\ 2 & \text{Quadratic patch test} \end{cases}$$
(63)

357 Table 1 lists the L_2 - and H_e -Error results of patch test with flat model, where
 358 the RKGSI scheme with variational consistent essential boundary enforcement,
 359 i.e. RKGSI-Nitsche and RKGSI-HW, can pass the linear and quadratic patch
 360 test. In contrast, the RKGSI-Penalty cannot pass the patch test since the
 361 Penalty method is unable to ensure the variational consistency. Due to the
 362 loss of variational consistency condition, even with the Nitsche's method, Gauss
 363 meshfree formulations show noticeable errors. Table 2 shows the results for
 364 curved model, which indicated that all the considered methods cannot pass

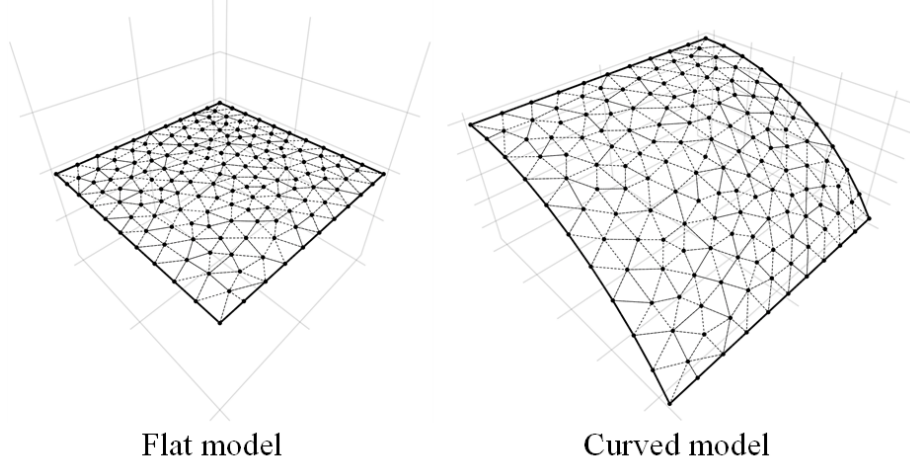


Figure 3: Meshfree discretization for patch test

365 the patch test. This is mainly because the proposed smoothed gradient of
 366 Eqs. (35) and (36) could not exactly reproduce the non-polynomial membrane
 367 and bending stresses. On the other hand, the RKGSI-HW and RKGSI-Nitsche
 368 methods provide better accuracy compared to the other approaches due to the
 369 fulfillment of first second-order variational consistency. Even only with local
 370 variational consistency, the RKGSI-Penalty obtained a better result than the
 371 traditional Gauss scheme. Meanwhile, the bending moment contours of M^{12}
 372 are listed in Fig. 4, which further verify that the proposed method provided a
 373 satisfactory result compared to the exact solution. Contrarily, both the RKGSI-
 374 Penalty and the conventional Gauss meshfree formulations observed errors.

Table 1: Results of patch test for flat model.

	Linear patch test		Quadratic patch test	
	L_2 -Error	H_e -Error	L_2 -Error	H_e -Error
GI-Penalty	$4.45E - 4$	$1.35E - 2$	$2.01E - 3$	$1.63E - 2$
GI-Nitsche	$4.51E - 4$	$1.42E - 2$	$1.22E - 3$	$1.68E - 2$
RKGSI-Penalty	$3.64E - 9$	$6.77E - 8$	$4.54E - 9$	$6.57E - 8$
RKGSI-Nitsche	$3.31E - 12$	$1.34E - 11$	$5.98E - 12$	$1.21E - 11$
RKGSI-HR	$6.67E - 13$	$1.50E - 11$	$1.07E - 12$	$1.26E - 11$

375 5.2. Scordelis-Lo roof

376 This example considers the classical Scordelis-Lo roof problem, as depicted
 377 in Fig. 5. The cylindrical roof has dimensions $R = 25$, $L = 50$, $h = 0.25$,
 378 Young's modulus $E = 4.32 \times 10^8$ and Poisson's ratio $\nu = 0.0$. The entire roof

Table 2: Results of patch test for cylindrical model.

	Linear patch test		Quadratic patch test	
	L_2 -Error	H_e -Error	L_2 -Error	H_e -Error
GI-Penalty	$3.79E - 4$	$1.30E - 2$	$1.74E - 3$	$1.37E - 2$
GI-Nitsche	$4.04E - 4$	$1.42E - 2$	$1.15E - 3$	$1.49E - 2$
RKGSI-Penalty	$1.47E - 4$	$5.39E - 3$	$2.26E - 4$	$2.09E - 3$
RKGSI-Nitsche	$2.41E - 6$	$7.37E - 5$	$2.47E - 6$	$2.89E - 5$
RKGSI-HR	$4.28E - 6$	$1.30E - 4$	$9.69E - 6$	$2.41E - 4$

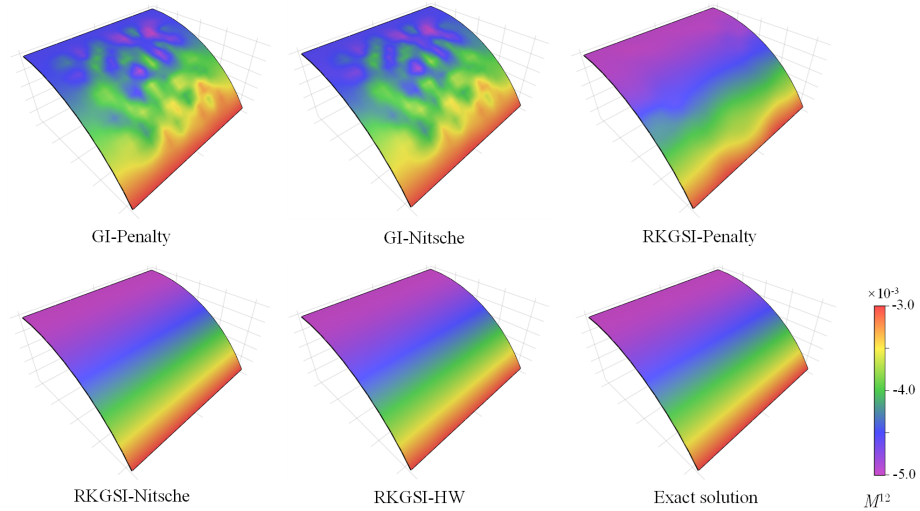


Figure 4: Contour plots of M^{12} for curved shell patch test.

is subjected to an uniform body force of $b_z = -90$, with the straight edges remainning free and the the curved edges are enforced by $v_x = v_z = 0$.

Due to the symmetry, only a quadrant of the model is considered for meshfree analysis, which is discretized by the 11×16 , 13×20 , 17×24 and 19×28 meshfree nodes, as listed in Fig. 6. The comparison of the displacement in z -direction at node A , v_{A3} , is used as the investigated quantity, with the reference value 0.3006 given by [33]. Firstly, Fig. 7 presents a sensitivity study for the artificial parameters of α_{vi} 's and α_θ 's in the RKGSI meshfree formulations with the Nitsche's and penalty- method, where all of the parameters are scaled by the support size as, $\alpha_{v\alpha} = s^{-1}\bar{\alpha}_v$, $\alpha_{v3} = s^{-3}\bar{\alpha}_v$ and $\alpha_\theta = s^{-1}\bar{\alpha}_\theta$. For a better comparison, the result of the proposed RKGSI-HW is also listed in this figure. The results of Fig. 7 revealed, that Nitsche's method observed less artificial sensitivity. However, both the methods cannot trivially determine the optimal values of the artificial parameters. The optimal artificial parameters from Fig. 7 are adopted for the convergence study in Fig. 8. The convergence result

³⁹⁴ showed that the RKGSI method get satisfactory results while the traditional
³⁹⁵ Gauss methods demonstrated noticeable errors.

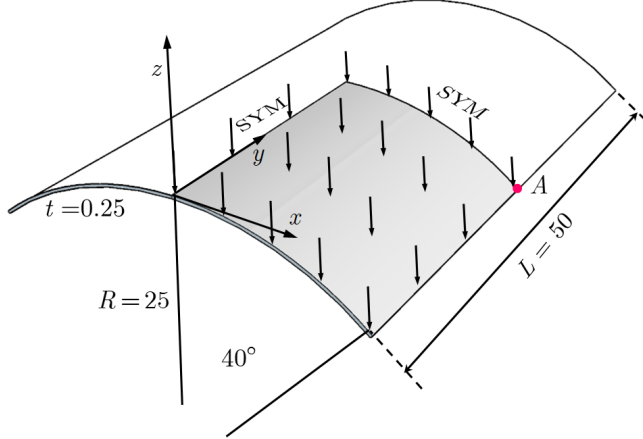


Figure 5: Description of Scordelis-Lo roof problem.

³⁹⁶ *5.3. Pinched Hemispherical shell*

³⁹⁷ Consider the hemispherical shell shown in Fig. 9, which is loaded at four
³⁹⁸ points $P = \pm 2$ at 90° interval at its bottom. The hemispherical shell has an
³⁹⁹ radius $R = 10$, thickness $h = 0.04$, Young's modulus $E = 6.825 \times 10^7$ and
⁴⁰⁰ Poisson's ratio $\nu = 0.3$.

⁴⁰¹ Due to symmetry, only quadrant model, where the 16×16 , 24×24 , 32×32
⁴⁰² and 40×40 meshfree nodes have been discretized as shown in Fig. (10), were con-
⁴⁰³ sidered. The quantity under investigation for convergence is the displacement
⁴⁰⁴ at x -direction on point A , v_{A1} . Fig. 11 displays the corresponding convergence
⁴⁰⁵ results, indicating the RKGSI scheme performed significantly better compared
⁴⁰⁶ to the GI meshfree formulation. Meanwhile, the efficiency comparison for this
⁴⁰⁷ problem is also shown in Fig. 12, in which the CPU time for the assembly
⁴⁰⁸ and calculation of shape functions are considered. Fig. 12(a) indicates that the
⁴⁰⁹ RKGSI scheme observed high efficiency in assembly. This is due to the vari-
⁴¹⁰ ational inconsistent Gauss meshfree formulation which require more Gaussian
⁴¹¹ points to achieve satisfactory results. Fig. 12(b) lists the CPU time spent on en-
⁴¹² forcing essential boundary conditions for the penalty-, Nitsche's- and proposed
⁴¹³ HW- methods. The results highlighted that the proposed HW method con-
⁴¹⁴ sumed comparable CPU time in the assembly compared to Nitsche's method.
⁴¹⁵ However, less time was spent to calculate the shape functions. Since both the
⁴¹⁶ HW- and penalty- method were developed considering the shape functions first
⁴¹⁷ order derivatives. For this reason, both the methods shared an almost identical
⁴¹⁸ time in computing the shape functions.

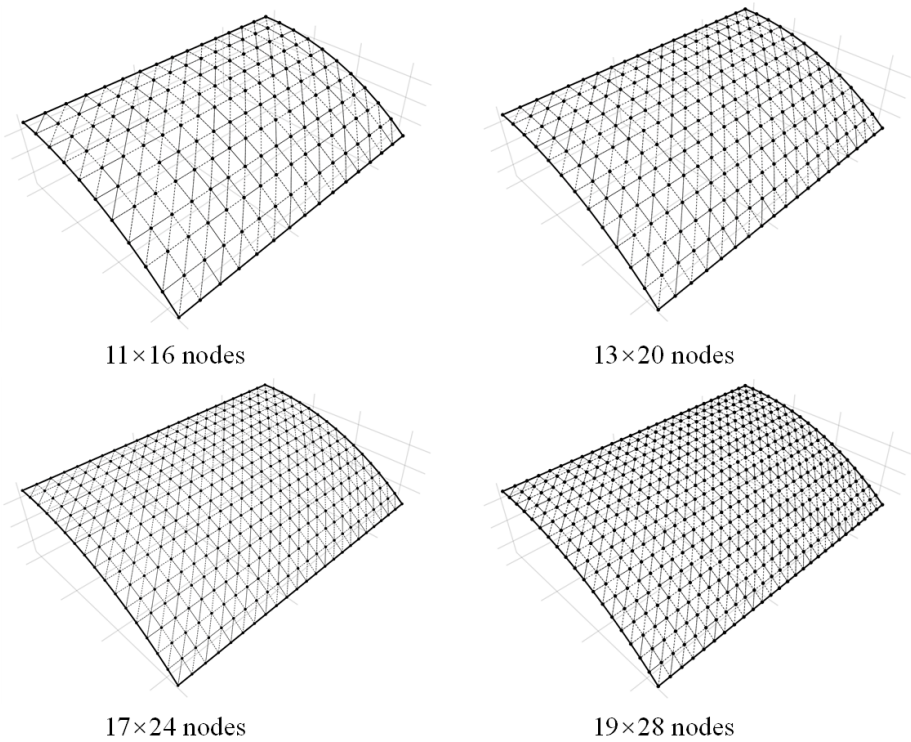
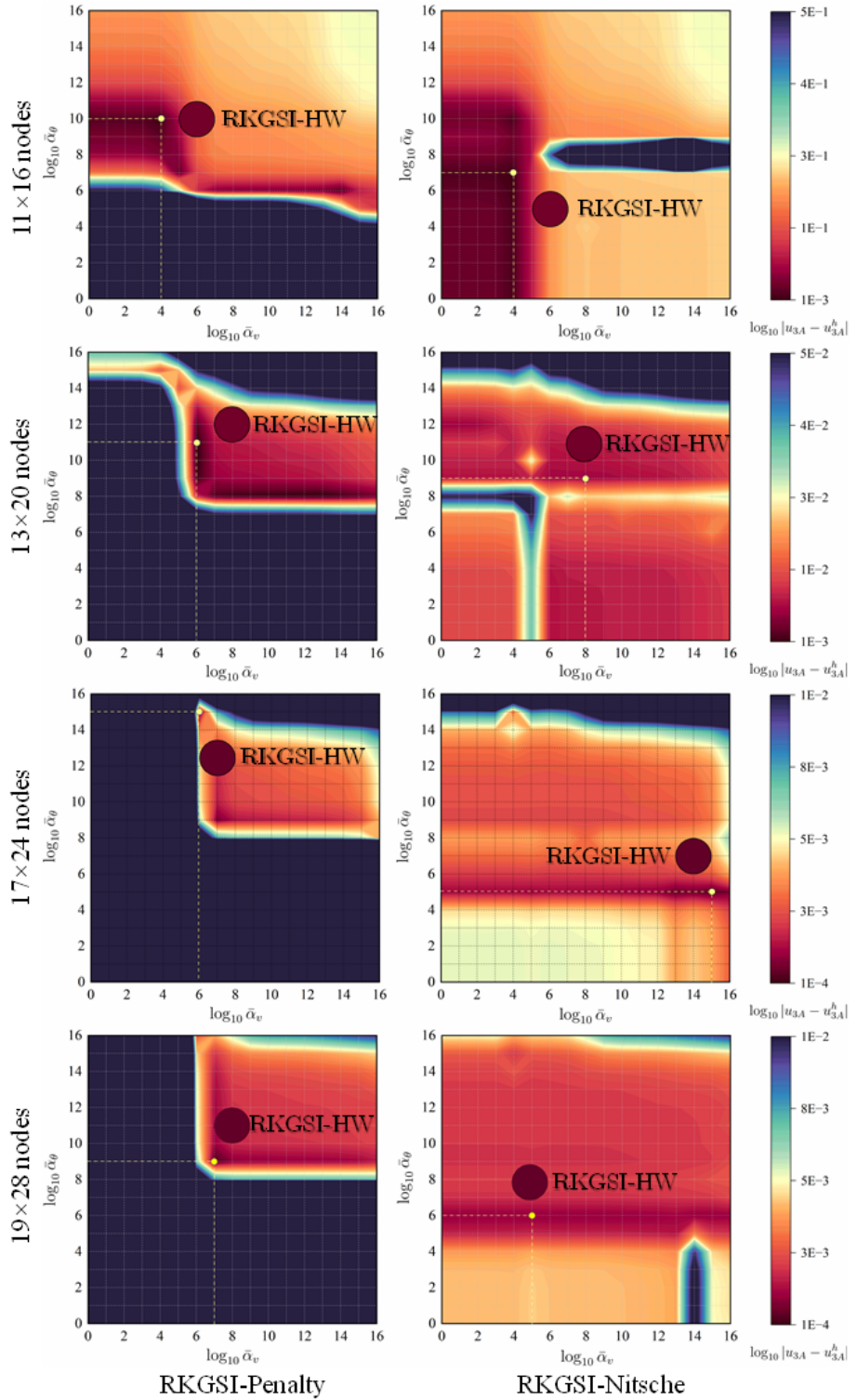


Figure 6: Meshfree discretizations for Scordelis-Lo roof problem.

Figure 7: Sensitivity comparison of α_v and α_θ for Scordelis-Lo problem.

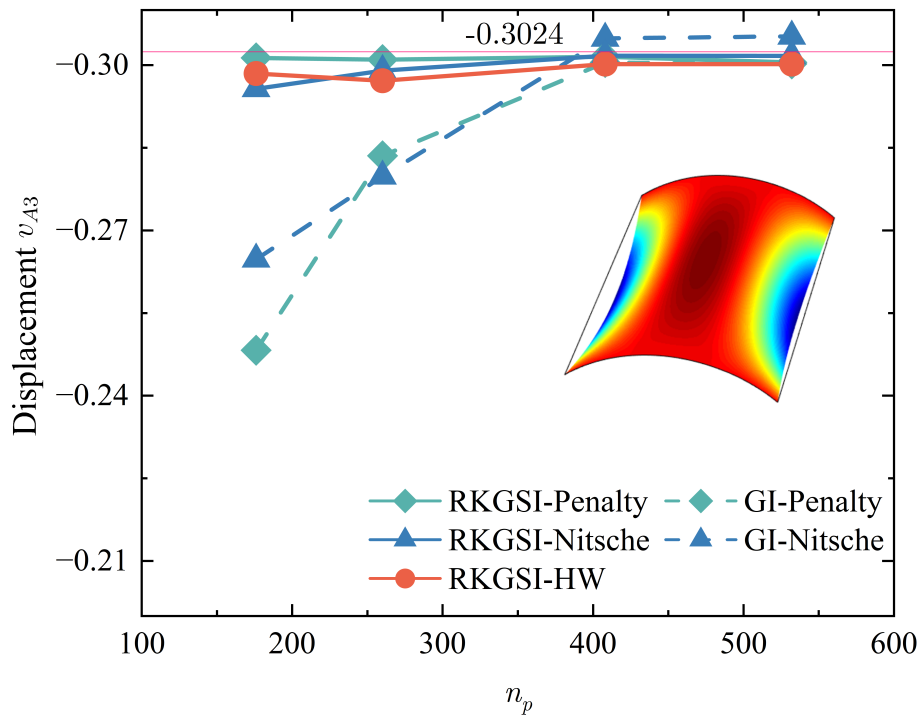


Figure 8: Displacement convergence for Scordelis-Lo roof problem.

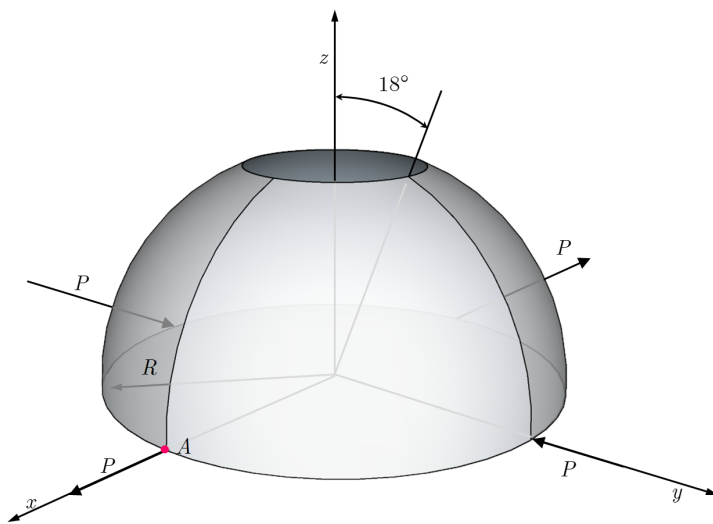


Figure 9: Description of pinched hemispherical shell problem.

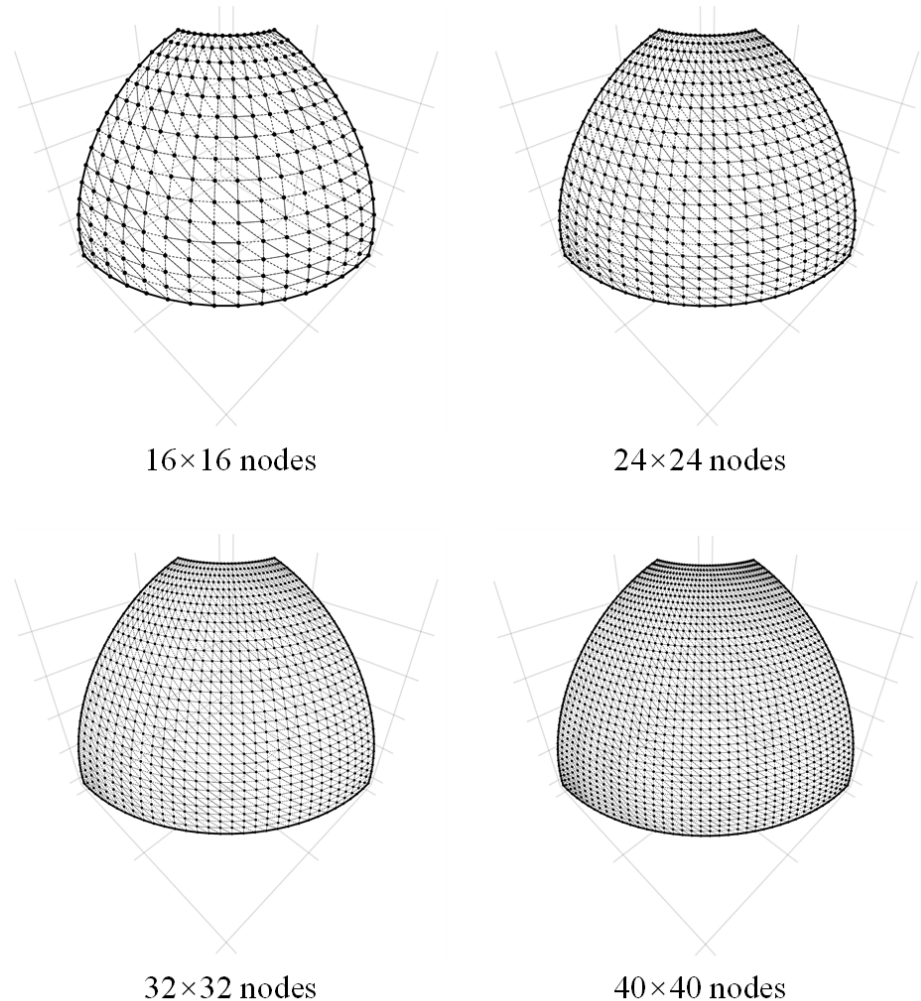


Figure 10: Meshfree discretizations for pinched hemispherical shell problem.

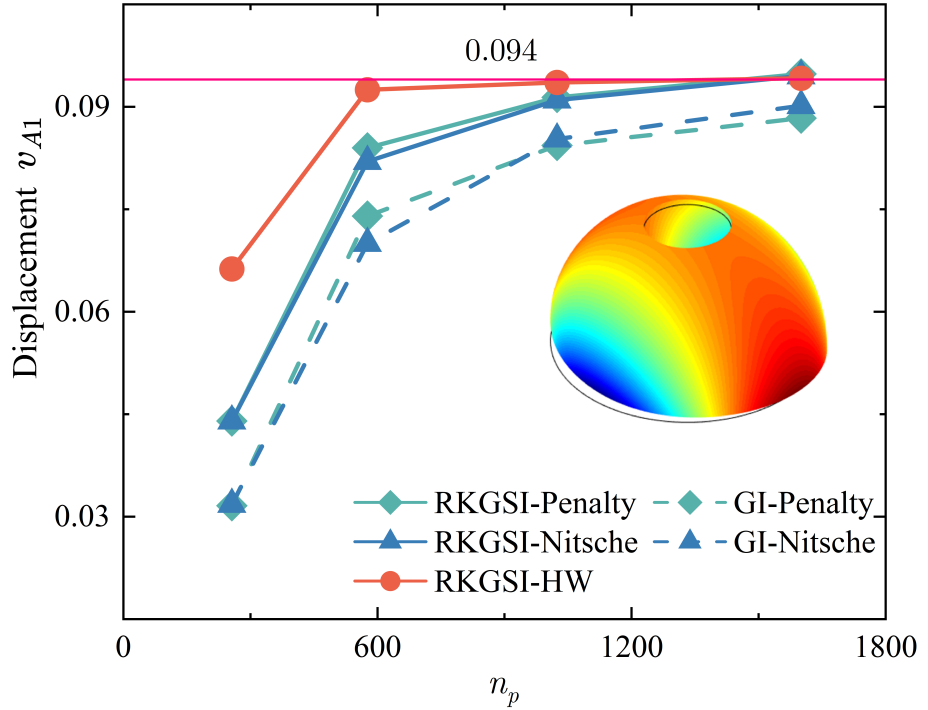


Figure 11: Displacement convergence for pinched hemispherical shell problem.

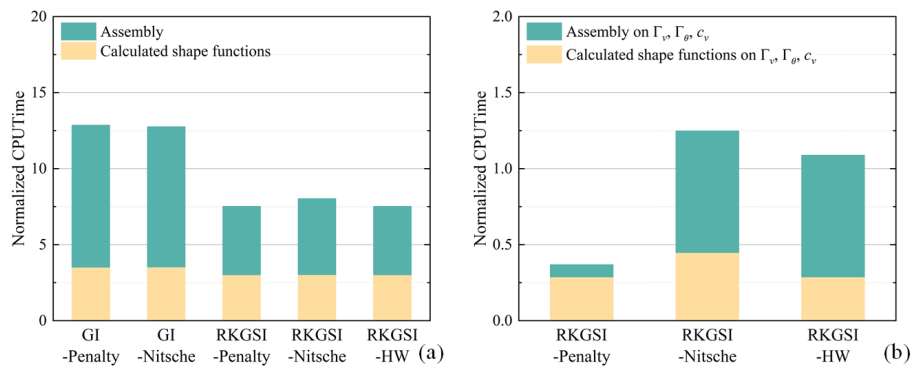


Figure 12: efficiency comparison for pinched hemispherical shell problem: (a) Whole domain; (b) Essential boundaries

419 **6. Conclusion**

420 In this study, an efficient and quasi-consistent meshfree thin shell formu-
421 lation was presented to naturally enforce the essential boundary conditions.
422 Mixed formulation with the Hu-Washizu principle weak form is adopted, where
423 the traditional meshfree shape functions discretized the displacement, and the
424 strains and stresses were expressed by the reproducing kernel smoothed gradi-
425 ents and the covariant smoothed gradients, respectively. The smoothed gradient
426 naturally embedded the first second-order integration constraints and has
427 a quasi variational consistency for the curved models in each integration cell.
428 Owing to the Hu-Washizu variational principle, the essential boundary condi-
429 tion enforcement has a similar form with the conventional Nitsche's method;
430 both have consistent and stabilized terms. The costly high order derivatives in
431 the Nitsche's consistent term have been replaced by the smoothed gradients,
432 which improved the computational speed due to the reproducing kernel gradi-
433 ent smoothing framework. Furthermore, the stabilized term naturally existed
434 in the Hu-Washizu weak form, and the artificial parameter needed in Nitsche's
435 stabilized term has vanished, which can automatically maintain the coercivity
436 for the stiffness matrix. Based on general reproducing kernel gradient smooth-
437 ing framework, the proposed methodology can be trivially extended to high
438 order basis meshfree formulation. The numerical results demonstrated that the
439 proposed Hu-Washizu quasi-consistent meshfree thin shell formulation showed
440 excellent accuracy, efficiency, and stability.

⁴⁴¹ **Acknowledgment**

⁴⁴² The support of this work by the National Natural Science Foundation of
⁴⁴³ China (12102138, 52350410467) and the Natural Science Foundation of Fujian
⁴⁴⁴ Province of China (2023J01108, 2022J05056) is gratefully acknowledged.

445 **Appendix A. Green's theorems for in-plane vector**

446 This Appendix discusses two kinds of Green's theorems used for the development
 447 of the proposed meshfree method. For an arbitrary vectors v^α and a
 448 scalar function f , with Green's theorem for in-plane vector, the first Green's
 449 theorem is listed as follows [30]:

$$\begin{aligned} \int_{\Omega} f_{,\alpha} v^\alpha d\Omega &= \int_{\Gamma} f v^\alpha n_\alpha d\Gamma - \int_{\Omega} f(v_{,\alpha}^\alpha + \Gamma_{\beta\alpha}^\beta v^\alpha) d\Omega \\ &= \int_{\Gamma} f v^\alpha n_\alpha d\Gamma - \int_{\Omega} f v^\alpha|_\alpha d\Omega \end{aligned} \quad (\text{A.1})$$

450 where $\Gamma_{\alpha\beta}^\gamma = \mathbf{a}_{\alpha,\beta} \cdot \mathbf{a}^\gamma$ denotes the Christoffel symbol of the second kind. $v^\alpha|_\alpha$
 451 can be represented as the in-plane covariant derivative of the vector v^α :

$$v^\alpha|_\alpha = v_{,\alpha}^\alpha + \Gamma_{\beta\alpha}^\beta v^\alpha \quad (\text{A.2})$$

452 The second Green's theorem is established with a mixed form of second
 453 order derivative. Let $A^{\alpha\beta}$ can be an arbitrary symmetric second order tensor,
 454 the Green's theorem yields [30]:

$$\begin{aligned} \int_{\Omega} f_{,\alpha}|_\beta A^{\alpha\beta} d\Omega &= \int_{\Gamma} f_{,\gamma} n^\gamma A^{\alpha\beta} n_\alpha n_\beta d\Gamma - \int_{\Gamma} f(A^{\alpha\beta} s_\alpha n_\beta)_{,\gamma} s^\gamma d\Gamma + [[f A^{\alpha\beta} s_\alpha n_\beta]]_{\mathbf{x}\in C} \\ &\quad - \int_{\Gamma} f(A_{,\beta}^{\alpha\beta} n_\alpha + \Gamma_{\alpha\beta}^\gamma A^{\alpha\beta} n_\gamma + \Gamma_{\gamma\beta}^\gamma A^{\alpha\beta} n_\alpha) d\Gamma \\ &\quad + \int_{\Omega} f \left(\begin{array}{l} \Gamma_{\alpha\beta,\gamma}^\gamma A^{\alpha\beta} + \Gamma_{\alpha\beta}^\gamma A^{\alpha\beta} + \Gamma_{\eta\gamma}^\eta \Gamma_{\alpha\beta}^\gamma A^{\alpha\beta} \\ + A_{,\alpha\beta}^{\alpha\beta} + \Gamma_{\gamma\beta,\alpha}^\gamma A^{\alpha\beta} + 2\Gamma_{\gamma\alpha}^\gamma A_{,\beta}^{\alpha\beta} + \Gamma_{\gamma\alpha}^\gamma \Gamma_{\eta\beta}^\eta A^{\alpha\beta} \end{array} \right) d\Omega \\ &= \int_{\Gamma} f_{,\gamma} n^\gamma A^{\alpha\beta} n_\alpha n_\beta d\Gamma - \int_{\Gamma} f(A^{\alpha\beta} s_\alpha n_\beta)_{,\gamma} s^\gamma d\Gamma + [[f A^{\alpha\beta} s_\alpha n_\beta]]_{\mathbf{x}\in C} \\ &\quad - \int_{\Gamma} f A^{\alpha\beta}|_\beta n_\alpha d\Gamma + \int_{\Omega} f A^{\alpha\beta}|_\alpha n_\beta d\Omega \end{aligned} \quad (\text{A.3})$$

455 with

$$A^{\alpha\beta}|_\beta = A_{,\beta}^{\alpha\beta} + \Gamma_{\beta\gamma}^\alpha A^{\beta\gamma} + \Gamma_{\gamma\beta}^\gamma A^{\alpha\beta} \quad (\text{A.4})$$

$$\begin{aligned} A^{\alpha\beta}|_{\alpha\beta} &= \Gamma_{\alpha\beta,\gamma}^\gamma A^{\alpha\beta} + \Gamma_{\alpha\beta}^\gamma A^{\alpha\beta} + \Gamma_{\eta\gamma}^\eta \Gamma_{\alpha\beta}^\gamma A^{\alpha\beta} \\ &\quad + A_{,\alpha\beta}^{\alpha\beta} + \Gamma_{\gamma\beta,\alpha}^\gamma A^{\alpha\beta} + 2\Gamma_{\gamma\alpha}^\gamma A_{,\beta}^{\alpha\beta} + \Gamma_{\gamma\alpha}^\gamma \Gamma_{\eta\beta}^\eta A^{\alpha\beta} \end{aligned} \quad (\text{A.5})$$

457 For the sake of brevity, the notion of covariant derivative is extended to a
 458 scalar function as:

$$f|_\alpha = f_{,\alpha} + \Gamma_{\beta\alpha}^\beta f \quad (\text{A.6})$$

$$f|_\beta n_\alpha = f_{,\beta} n_\alpha + \Gamma_{\alpha\beta}^\gamma f n_\gamma + \Gamma_{\gamma\beta}^\gamma f n_\alpha \quad (\text{A.7})$$

$$\begin{aligned} f|_{\alpha\beta} &= \Gamma_{\alpha\beta,\gamma}^\gamma f + \Gamma_{\alpha\beta}^\gamma f_{,\gamma} + \Gamma_{\eta\gamma}^\eta \Gamma_{\alpha\beta}^\gamma f \\ &\quad + f_{,\alpha\beta} + \Gamma_{\gamma\beta,\alpha}^\gamma f + 2\Gamma_{\gamma\alpha}^\gamma f_{,\beta} + \Gamma_{\gamma\alpha}^\gamma \Gamma_{\eta\beta}^\eta f \end{aligned} \quad (\text{A.8})$$

⁴⁶¹ **Appendix B. Derivations for stiffness metrics and force vectors**

⁴⁶² This Appendix details the derivations of stiffness matrices and force vectors
⁴⁶³ in Eqs. (53)-(55), where the relationships of Eqs. (40), (41), (44) and (46) are
⁴⁶⁴ used herein. Firstly, the membrane strain terms are considered as follows:

$$\begin{aligned}
 & \sum_{C=1}^{n_e} \int_{\Omega_C} \delta \tilde{\varepsilon}_{\alpha\beta}^h h C^{\alpha\beta\gamma\eta} \tilde{\varepsilon}_{\gamma\eta}^h d\Omega \\
 &= \sum_{C=1}^{n_e} \sum_{I,J=1}^{n_p} \delta \mathbf{d}_I \cdot \underbrace{\int_{\Omega_C} \tilde{\varepsilon}_{\alpha\beta I} h C^{\alpha\beta\gamma\eta} \mathbf{a}_\gamma \mathbf{q}^T d\Omega \mathbf{G}^{-1} \bar{\mathbf{g}}_{\eta J} \cdot \mathbf{d}_J}_{\tilde{\mathbf{g}}_I^{\eta T}} \\
 &= \sum_{C=1}^{n_e} \sum_{I,J=1}^{n_p} \delta \mathbf{d}_I \cdot \underbrace{\int_{\Gamma_C \cap \Gamma_v} \Psi_J \mathbf{q}^T \mathbf{G}^{-1} \tilde{\mathbf{g}}_I^\alpha n_\alpha d\Gamma}_{\tilde{\mathbf{T}}_{NI}} \cdot \mathbf{d}_J \\
 &= \sum_{I,J=1}^{n_p} \delta \mathbf{d}_I \cdot \int_{\Gamma_v} \tilde{\mathbf{T}}_{NI} \Psi_J d\Gamma \cdot \mathbf{d}_J
 \end{aligned} \tag{B.1}$$

⁴⁶⁵ with

$$\tilde{\mathbf{g}}_I^\alpha = \mathbf{q} \mathbf{a}_\beta h C^{\alpha\beta\gamma\eta} \tilde{\varepsilon}_{\gamma\eta I} \tag{B.2}$$

$$\tilde{\mathbf{T}}_{NI} = \mathbf{q}^T \mathbf{G}^{-1} \tilde{\mathbf{g}}_I^\alpha n_\alpha \tag{B.3}$$

⁴⁶⁷ Following this path, the bending strain terms can be reorganized by:

$$\begin{aligned}
 & \sum_{C=1}^{n_e} \int_{\Omega_C} \delta \tilde{\kappa}_{\alpha\beta}^h \frac{h^3}{12} C^{\alpha\beta\gamma\eta} \tilde{\kappa}_{\gamma\eta}^h d\Omega \\
 &= \sum_{C=1}^{n_e} \sum_{I,J=1}^{n_p} \delta \mathbf{d}_I \cdot \underbrace{\int_{\Omega_C} \tilde{\kappa}_{\alpha\beta I} \frac{h^3}{12} C^{\alpha\beta\gamma\eta} \mathbf{a}_3 \mathbf{q}^T d\Omega \mathbf{G}^{-1} \bar{\mathbf{g}}_{\gamma\eta J} \cdot \mathbf{d}_J}_{\tilde{\mathbf{g}}_I^{\gamma\eta T}} \\
 &= \sum_{C=1}^{n_e} \sum_{I,J=1}^{n_p} \delta \mathbf{d}_I \cdot \left(\begin{array}{l} \int_{\Gamma_C \cap \Gamma_\theta} \underbrace{\mathbf{q}^T \mathbf{G}^{-1} \tilde{\mathbf{g}}_I^{\alpha\beta} n_\alpha n_\beta}_{\tilde{\mathbf{M}}_{nnI}} n^\gamma \Psi_{J,\gamma} d\Gamma \\ - \int_{\Gamma_C \cap \Gamma_v} \underbrace{(\mathbf{q}_{\beta}^T \mathbf{G}^{-1} \tilde{\mathbf{g}}_I^{\alpha\beta} n_\alpha + (\mathbf{q}^T \mathbf{G}^{-1} \tilde{\mathbf{g}}_I^{\alpha\beta} s_\alpha n_\beta)_{,\gamma} s^\gamma)}_{\tilde{\mathbf{T}}_{MI}} \Psi_J d\Gamma \\ + [[\underbrace{\mathbf{q}^T \mathbf{G}^{-1} \tilde{\mathbf{g}}_I^{\alpha\beta} s_\alpha n_\beta}_{\tilde{\mathbf{P}}_I \mathbf{a}_3} \Psi_J]]_{\mathbf{x} \in C_C \cap C_v} \end{array} \right) \cdot \mathbf{d}_J \\
 &= \sum_{I,J=1}^{n_p} \delta \mathbf{d}_I \cdot \left(\int_{\Gamma_\theta} \tilde{\mathbf{M}}_{nnI} n^\gamma \Psi_{J,\gamma} d\Gamma - \int_{\Gamma_v} \tilde{\mathbf{T}}_{MI} \Psi_J d\Gamma + [[\tilde{\mathbf{P}}_I \Psi_J]]_{\mathbf{x} \in C_v} \right)
 \end{aligned} \tag{B.4}$$

⁴⁶⁸ with

$$\tilde{\mathbf{g}}_I^{\alpha\beta} = \int_{\Omega_C} \mathbf{q} \frac{h^3}{12} C^{\alpha\beta\gamma\eta} \mathbf{a}_3 \tilde{\boldsymbol{\kappa}}_{\gamma\eta I} d\Omega \quad (\text{B.5})$$

⁴⁶⁹

$$\begin{cases} \tilde{M}_{nnI} = \mathbf{q}^T \mathbf{G}^{-1} \tilde{\mathbf{g}}_I^{\alpha\beta} n_\alpha n_\beta \\ \tilde{T}_{MI} = \mathbf{q}_{|\beta}^T \mathbf{G}^{-1} \tilde{\mathbf{g}}_I^{\alpha\beta} n_\alpha + (\mathbf{q}^T \mathbf{G}^{-1} \tilde{\mathbf{g}}_I^{\alpha\beta} s_\alpha n_\beta)_{,\gamma} s^\gamma \\ \tilde{P}_I = \mathbf{q}^T \mathbf{G}^{-1} \tilde{\mathbf{g}}_I^{\alpha\beta} s_\alpha n_\beta \cdot \mathbf{a}_3 \end{cases} \quad (\text{B.6})$$

470 **References**

- 471 [1] L. H. Donnell, Beams, Plates and Shells, McGraw-Hill, 1976.
- 472 [2] T. J. Hughes, The Finite Element Method: Linear Static and Dynamic
473 Finite Element Analysis, Dover Publications, Mineola, New York, 2000.
- 474 [3] T. Belytschko, Y. Y. Lu, L. Gu, Element-free Galerkin methods, International
475 Journal for Numerical Methods in Engineering 37 (1994) 229–256.
- 476 [4] W. K. Liu, S. Jun, Y. F. Zhang, Reproducing kernel particle methods,
477 International Journal for Numerical Methods in Fluids 20 (1995) 1081–
478 1106.
- 479 [5] J. S. Chen, M. Hillman, S. W. Chi, Meshfree methods: Progress made after
480 20 Years, Journal of Engineering Mechanics 143 (2017) 04017001.
- 481 [6] P. Krysl, T. Belytschko, Analysis of thin shells by the Element-Free
482 Galerkin method, International Journal of Solids and Structures 33 (1996)
483 3057–3080.
- 484 [7] G. R. Liu, Meshfree Methods: Moving Beyond the Finite Element Method,
485 Second Edition, Crc Press, 2009.
- 486 [8] X. Zhang, K. Z. Song, M. W. Lu, X. Liu, Meshless methods based on
487 collocation with radial basis functions, Computational Mechanics 26 (2000)
488 333–343.
- 489 [9] D. Millán, A. Rosolen, M. Arroyo, Thin shell analysis from scattered points
490 with maximum-entropy approximants, International Journal for Numerical
491 Methods in Engineering 85 (2011) 723–751.
- 492 [10] L. Wang, M. Hu, Z. Zhong, F. Yang, Stabilized Lagrange Interpolation
493 Collocation Method: A meshfree method incorporating the advantages of
494 finite element method, Computer Methods in Applied Mechanics and En-
495 gineering 404 (2023) 115780.
- 496 [11] P. Suchde, T. Jacquemin, O. Davydov, Point Cloud Generation for Mesh-
497 free Methods: An Overview, Archives of Computational Methods in Engi-
498 neering 30 (2022) 889–915.
- 499 [12] L. Deng, D. Wang, An accuracy analysis framework for meshfree collocation
500 methods with particular emphasis on boundary effects, Computer Methods
501 in Applied Mechanics and Engineering 404 (2023) 115782.
- 502 [13] J. Wang, M. Hillman, Upwind reproducing kernel collocation method for
503 convection-dominated problems, Computer Methods in Applied Mechanics
504 and Engineering 420 (2024) 116711.

- 505 [14] S. Fernández-Méndez, A. Huerta, Imposing essential boundary conditions
 506 in mesh-free methods, Computer Methods in Applied Mechanics and En-
 507 gineering 193 (2004) 1257–1275.
- 508 [15] X. Li, Error estimates for the moving least-square approximation and the
 509 element-free Galerkin method in n-dimensional spaces, Applied Numerical
 510 Mathematics 99 (2016) 77–97.
- 511 [16] J. Wu, D. Wang, An accuracy analysis of Galerkin meshfree methods ac-
 512 counting for numerical integration, Computer Methods in Applied Mechan-
 513 ics and Engineering 375 (2021) 113631.
- 514 [17] J. S. Chen, H. P. Wang, New boundary condition treatments in meshfree
 515 computation of contact problems, Computer Methods in Applied Mechan-
 516 ics and Engineering 187 (2000) 441–468.
- 517 [18] D. Liu, Y. M. Cheng, The interpolating element-free Galerkin (IEFG)
 518 method for three-dimensional potential problems, Engineering Analysis
 519 with Boundary Elements 108 (2019) 115–123.
- 520 [19] V. Ivannikov, C. Tiago, P. M. Pimenta, On the boundary conditions of the
 521 geometrically nonlinear Kirchhoff–Love shell theory, International Journal
 522 of Solids and Structures 51 (2014) 3101–3112.
- 523 [20] Y. Y. Lu, T. Belytschko, L. Gu, A new implementation of the element free
 524 Galerkin method, Computer Methods in Applied Mechanics and Engineer-
 525 ing 113 (1994) 397–414.
- 526 [21] T. Zhu, S. N. Atluri, A modified collocation method and a penalty formu-
 527 lation for enforcing the essential boundary conditions in the element free
 528 Galerkin method, Computational Mechanics 21 (1998) 211–222.
- 529 [22] S. Skatulla, C. Sansour, Essential boundary conditions in meshfree methods
 530 via a modified variational principle: Applications to shell computations,
 531 Computer Assisted Mechanics and Engineering Sciences 15 (2008) 123–142.
- 532 [23] J. S. Chen, C. T. Wu, S. Yoon, Y. You, A stabilized conforming nodal
 533 integration for Galerkin mesh-free methods, International Journal for Nu-
 534 matical Methods in Engineering 50 (2001) 435–466.
- 535 [24] J. S. Chen, M. Hillman, M. Rüter, An arbitrary order variationally consis-
 536 tent integration for Galerkin meshfree methods, International Journal for
 537 Numerical Methods in Engineering 95 (2013) 387–418.
- 538 [25] Q. Duan, X. Li, H. Zhang, T. Belytschko, Second-order accurate derivatives
 539 and integration schemes for meshfree methods, International Journal for
 540 Numerical Methods in Engineering 92 (2012) 399–424.

- 541 [26] D. Wang, J. Wu, An inherently consistent reproducing kernel gradient
542 smoothing framework toward efficient Galerkin meshfree formulation with
543 explicit quadrature, Computer Methods in Applied Mechanics and Engi-
544 neering 349 (2019) 628–672.
- 545 [27] J. Wang, X. Ren, A consistent projection integration for Galerkin meshfree
546 methods, Computer Methods in Applied Mechanics and Engineering 414
547 (2023) 116143.
- 548 [28] J. Wu, X. Wu, Y. Zhao, D. Wang, A consistent and efficient method for
549 imposing meshfree essential boundary conditions via hellinger-reissner vari-
550 ational principle., Chinese Journal of Theoretical and Applied Mechanics
551 54 (2022) 3283–3296.
- 552 [29] J. Wu, X. Wu, Y. Zhao, D. Wang, A rotation-free Hellinger-Reissner mesh-
553 free thin plate formulation naturally accommodating essential boundary
554 conditions, Engineering Analysis with Boundary Elements 154 (2023) 122–
555 140.
- 556 [30] J. Benzaken, J. A. Evans, S. F. McCormick, R. Tamstorf, Nitsche’s method
557 for linear Kirchhoff–Love shells: Formulation, error analysis, and verifica-
558 tion, Computer Methods in Applied Mechanics and Engineering 374 (2021)
559 113544.
- 560 [31] H. Dah-wei, A method for establishing generalized variational principle,
561 Applied Mathematics and Mechanics 6 (1985) 501–509.
- 562 [32] H. Du, J. Wu, D. Wang, J. Chen, A unified reproducing kernel gradient
563 smoothing Galerkin meshfree approach to strain gradient elasticity, Com-
564 putational Mechanics 70 (2022) 73–100.
- 565 [33] J. Kiendl, K. U. Bletzinger, J. Linhard, R. Wüchner, Isogeometric shell
566 analysis with Kirchhoff–Love elements, Computer Methods in Applied Me-
567 chanics and Engineering 198 (2009) 3902–3914.